KfK 5247
Oktober 1993

Fully Developed Magnetohydrodynamic Flows in Rectangular Ducts with Insulating Walls

S. Molokov, A. Shishko
Institut für Angewandte Thermo- und Fluiddynamik
Projekt Kernfusion

Kernforschungszentrum Karlsruhe

Kernforschungszentrum Karlsruhe
Institut für Angewandte Thermo- und Fluiddynamik
Projekt Kernfusion

KfK 5247

Fully Developed Magnetohydrodynamic Flows in Rectangular Ducts with Insulating Walls

S. Molokov and A. Shishko*

*** Latvian Academy of Sciences, Institute of Physics, Salaspils, Latvia**

Kernforschungszentrum Karlsruhe GmbH, Karlsruhe

Kernforschungszentrum Karlsruhe GmbH
Postfach 3640, 76021 Karlsruhe

ISSN 0303-4003

Abstract

Fully developed magnetohydrodynamic flows in rectangular ducts with insulating and semi-insulating walls (electrically conducting walls covered by insulating coatings) are considered. The report consists of two parts. In the first part the effect of magnetic field inclination on the flow structure and the pressure drop is considered. The duct walls are insulating. An asymptotic solution to the problem at high Hartmann numbers is obtained. The results show that for a square duct the increase of the pressure gradient due to the field inclination is negligible (less than 10 per cent for any angle). For blanket relevant values of inclination of up to 10^{o} the deviation of the velocity profile from the slug profile is insignificant. The second part studies the flow in a duct with insulating walls parallel to the magnetic field, while the Hartmann walls are covered by an insulating coating. A new type of the boundary condition is derived, which takes into account finite coating resistance. The effect of the latter on the flow characteristics is studied. An exact solution to the problem is obtained and several approximate formulas for the pressure drop at high Hartmann numbers are presented.

Voll ausgebildete magnetohydrodynamische Strömungen in Rechteckkanälen mit isolierten Wänden

Zusammenfassung

In diesem Bericht werden voll ausgebildete MHD-Strömungen in Rechteckkanälen mit isolierten und halb isolierten Wänden (elektrisch leitende Wände sind mit einer Isolationsschicht überzogen) betrachtet. Der Bericht besteht aus zwei Teilen. Im ersten Teil wird der Einfluß der Magnetfeldneigung auf die Strömungsform und den Druckverlust betrachtet. Die Kanalwände sind isoliert. Für große Hartmann- Zahlen wird eine asymptotische Lösung des Problems hergeleitet. Die Ergebnisse zeigen, daß für einen quadratischen Kanal die Erhöhung des Druckverlusts aufgrund der Magnetfeldneigung vernachlässigbar ist (weniger als 10% für beliebige Winkel). Für blanket- relevante Neigungen bis 10^o ist die Abweichung des Geschwindigkeitsprofils vom kolbenförmigen Profil nur unbedeutend. Im zweiten Teil wird eine Strömung in einem Kanal untersucht, dessen Wände parallel zum Magnetfeld isoliert sind, während die Hartmann- Wände mit einer Isolationsschicht überzogen sind. Es wird eine neue Randbedingung hergeleitet, die einen endlichen Widerstand der Beschichtung berücksichtigt. Ihr Einfluß auf die Strömungsformen wird untersucht. Es wird eine exakte Lösung des Problems entwickelt. Für große Hartmann- Zahlen werden mehrere Näherungsformeln für den Druckverlust angegeben.

Contents

1. Introduction

Flows in ducts with insulating or semi-insulating walls are currently on agenda due to new trends in blanket-relevant research for DEMO and ITER. In several designs of poloidal self-cooled liquid-metal blankets the ducts are either fully insulated or have conducting walls, which are covered by insulating coatings. In poloidal concepts of blankets, such as those presented by Lavrentiev (1990), Sze *et al.* (1992) and Malang *et al.* (1993) the major part of flow is either fully developed or very close to it (quasi fully developed). The liquid metal flows in a strong transverse magnetic field, the main component of which is toroidal. If the field is perfectly aligned with one pair of the duct walls, the velocity profile is the slug one (Shercliff, 1953, Temperley, 1976). However, the actual magnetic field is three-dimensional, since the other two components of the plasma confining magnetic field are non-zero. The effect of magnetic field inclination on the flow in a rectangular duct with insulating walls is studied in the first part of the report (§2).

The second part (§ 3) studies the effect of finite resistance of an insulating coating and the aspect ratio of the rectangular channel on the flow structure and the pressure drop. The required insulating properties of the coating have recently been discussed by Bühler & Molokov (1993).

The results presented in this report were obtained by the authors in the period 1987-1989, but have never been published previously (the results of the first part were presented at the 13^{th} Riga Conference on Magnetohydrodynamics, see Molokov, 1990). This work was done for the former Soviet, presently Russian, concept of the slotted channel self-cooled liquid-metal blanket (see Lavrentiev, 1990). Promising results for insulating materials for this concept were obtained already at that time. Since the aspect ratio of the channels is arbitrary, the results presented here are valid for any poloidal blanket concept.

2. The effect of a magnetic field inclination

2. 1 Problem formulation

Consider the steady flow of a viscous, conducting fluid along the x_*-axis in an insulating rectangular channel of constant cross-section in the presence of a strong, uniform, transverse magnetic field

$$\underline{B}^e = B_0\left[\sin\theta \underline{e}_y + \cos\theta \underline{e}_z\right], \tag{2.1}$$

which is inclined with respect to the z_*-axis by the angle of θ (figure 2.1).

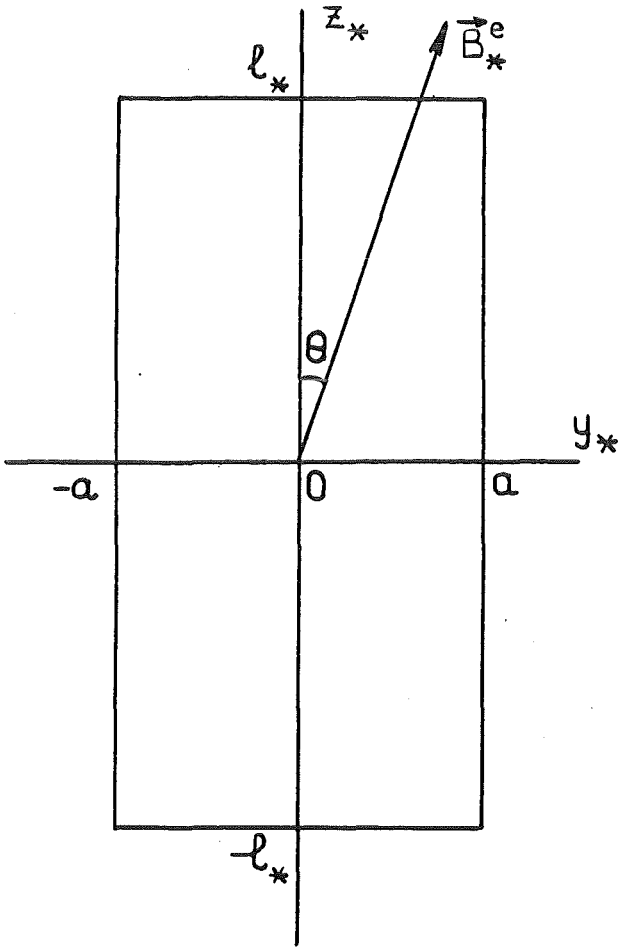

Fig. 2. 1 Flow in a rectangular channel in a skewed magnetic field

The equations governing the flow in the magnetic field (2.1) are (e.g. Shercliff, 1965)

$$\Delta_* v_* + \frac{B_0}{\rho \nu \mu_0}\left[\sin\theta \frac{\partial b_*}{\partial y_*} + \cos\theta \frac{\partial b_*}{\partial z_*}\right] = -\frac{k_*}{\rho \nu}, \tag{2.2}$$

$$\Delta_* b_* + \mu_0 \sigma B_0 \left[\sin\theta \frac{\partial v_*}{\partial y_*} + \cos\theta \frac{\partial v_*}{\partial z_*}\right] = 0, \tag{2.3}$$

where $v_* = v_{x_*}(y_*, z_*)$ is the fluid velocity, $b_* = b_{x_*}(y_*, z_*)$ is the induced magnetic field, ν is the kinematic viscosity, ρ is the density, σ is the electrical conductivity of the fluid, μ_0 is the magnetic permeability, k_* is the absolute value of the constant pressure gradient, $\Delta_* = \partial^2/\partial y_*^2 + \partial^2/\partial z_*^2$.

The dimensionless variables are introduced by scaling the length, the fluid velocity, the induced magnetic field and the pressure by the characteristic values of a, v_0 (average fluid velocity), $\mu_0 v_0 \sqrt{\rho \nu \sigma}$ and $\nu \rho v_0 / a$, respectively. Then the equations (2.2), (2.3) read

$$\Delta v + M\left[\sin\theta \frac{\partial b}{\partial y} + \cos\theta \frac{\partial b}{\partial z}\right] = -k, \tag{2.4}$$

$$\Delta b + M\left[\sin\theta \frac{\partial v}{\partial y} + \cos\theta \frac{\partial v}{\partial z}\right] = 0, \tag{2.5}$$

where $M = B_0 a \sqrt{\sigma/\rho\nu}$ is the Hartmann number. The notation of the dimensionless variables is the same as that of dimensional ones omitting asterisks.

The boundary conditions are

$$v = 0, \quad b = 0 \qquad \text{at } y = \pm 1, \tag{2.6}$$

$$v = 0, \quad b = 0 \qquad \text{at } z = \pm l. \tag{2.7}$$

In addition, the average fluid velocity in the channel cross-section is constant, so that

$$v_{av} = \frac{1}{4l}\int_{-1}^{1} dy \int_{-l}^{l} v(y,z)dz = 1. \tag{2.8}$$

For the problem considered an exact solution exists (see Vatazhin, Liubimov & Regirer, 1970 and references there). However, the analysis of this solution at high M is difficult.

The equations (2.4) and (2.5) contain a small parameter M^{-1} at the Laplacians, so that the problem (2.4) - (2.7) is that of singular perturbations. In the present report an asymptotic solution to this problem as $M \to \infty$ is presented.

The problem of flow in an insulating rectangular channel in the magnetic field parallel to a pair of walls ($\theta = 0$ or $\frac{\pi}{2}$) was treated by Temperley (1976). It is well known that at the walls parallel to the field side layers appear with the thickness $O\left(M^{-1/2}\right)$. The fluid velocity in the layers is $O(1)$. When the field inclination is small ($\theta = O\left(M^{-1/2}\right)$ or $\theta = \frac{\pi}{2} - O\left(M^{-1/2}\right)$) the flow structure is almost the same as for $\theta = 0$ and the side layers remain attached to the side walls. If inclination is significant ($\tan\theta = O(1)$) the side boundary layers separate from the walls and become free layers. They occur inside the fluid along magnetic field lines, which cross the channel corners. Thus the analysis will be carried out for the most interesting case $\tan\theta = O(1)$ for three different situations

i) $\tan\theta < l^{-1}$,

ii) $\tan\theta = l^{-1}$,

iii) $\tan\theta > l^{-1}$.

2. 2 *Asymptotic solution for* $\tan\theta < l^{-1}$

It is convenient to introduce new independent variables ξ and η as follows

$$\xi = y\cos\theta - z\sin\theta, \tag{2.9}$$

$$\eta = y\sin\theta + z\cos\theta. \tag{2.10}$$

The axis $O\eta$ is aligned with the magnetic field, while the axis $O\xi$ is in the transverse direction (see figure 2.2).

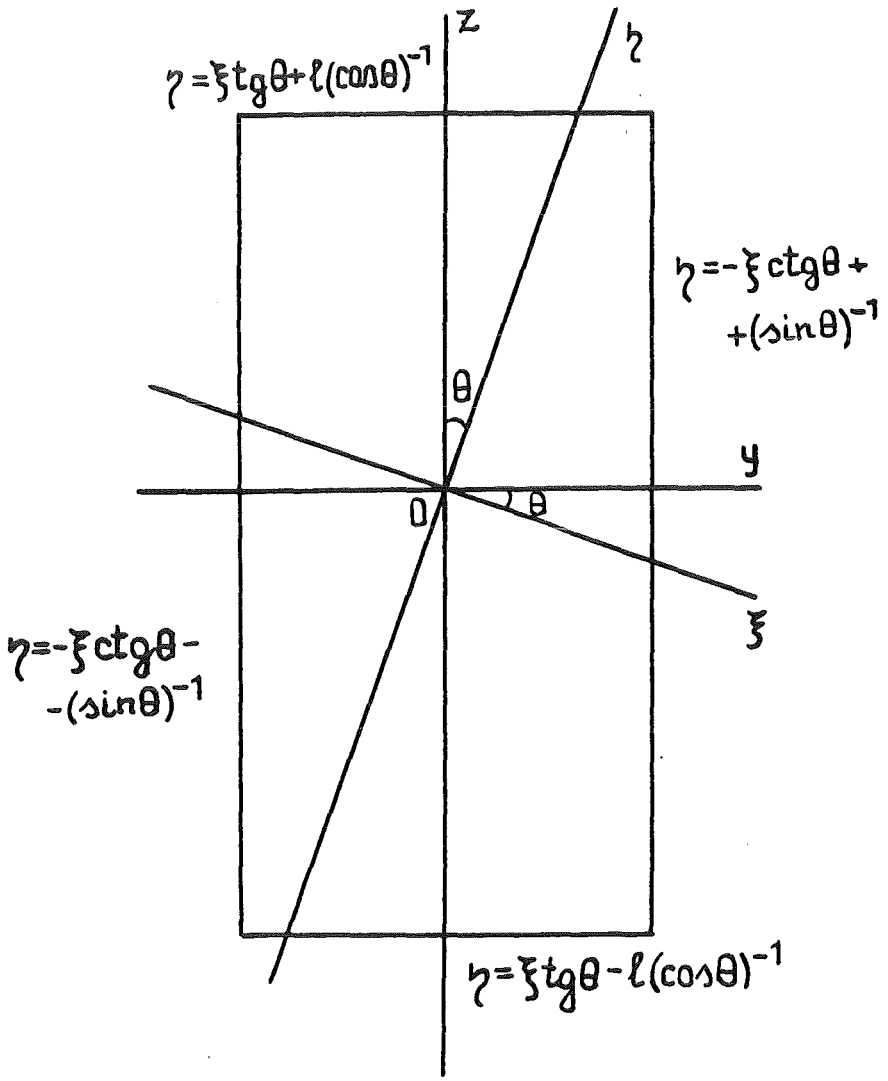

Fig. 2. 2 Channel cross-section and co-ordinate system $\xi O\eta$

In new variables the problem (2.4) - (2.7) reads

$$\Delta_1 v + M\frac{\partial b}{\partial \eta} = -k, \qquad \Delta_1 b + M\frac{\partial v}{\partial \eta} = 0, \tag{2.11}$$

$$v = 0, \quad b = 0 \qquad \text{at } \eta = -\xi\cot\theta \pm \frac{1}{\sin\theta}, \tag{2.12}$$

$$v = 0, \quad b = 0 \qquad \text{at } \eta = \xi\tan\theta \pm \frac{l}{\cos\theta}, \tag{2.13}$$

where $\Delta_1 = \partial^2/\partial\xi^2 + \partial^2/\partial\eta^2$.

According to the method of matched asymptotic expansions the flow region is divided into the following subregions (see figure 2.3):

- (CC) the central core between the walls $z = \pm l$,
- (LC) the left core between the walls $y=-1$ and $z=l$,
- (RC) the right core between the walls $z=-l$ and $y=l$,
- (HCL), (HCU) the Hartmann layers adjacent to the central core. They are at the walls $z=-l$ and $z=l$ and have thickness $O\left(|\cos\theta|M^{-1}\right)$,
- (HLL), (HLU) the Hartmann layers adjacent to the left core. They are at the walls $y=-1$ and $z=l$ and have thickness $O\left(|\sin\theta|M^{-1}\right)$ and $O\left(|\cos\theta|M^{-1}\right)$, respectively,
- (HRL), (HRU) the Hartmann layers adjacent to the right core. They are at the walls $z=-l$ and $y=l$ and have thickness $O\left(|\cos\theta|M^{-1}\right)$ and $O\left(|\sin\theta|M^{-1}\right)$, respectively,
- (SL) free layer of thickness $O\left(M^{-1/2}\right)$ separating the central and the left cores,
- (SR) free layer of thickness $O\left(M^{-1/2}\right)$ separating the central and the right cores,
- (HS1)-(HS4) Hartmann boundary layers adjacent to the layer SL,

- (HS5)-(HS8) Hartmann boundary layers adjacent to the layer SR,
- (I1)-(I4) corner layers.

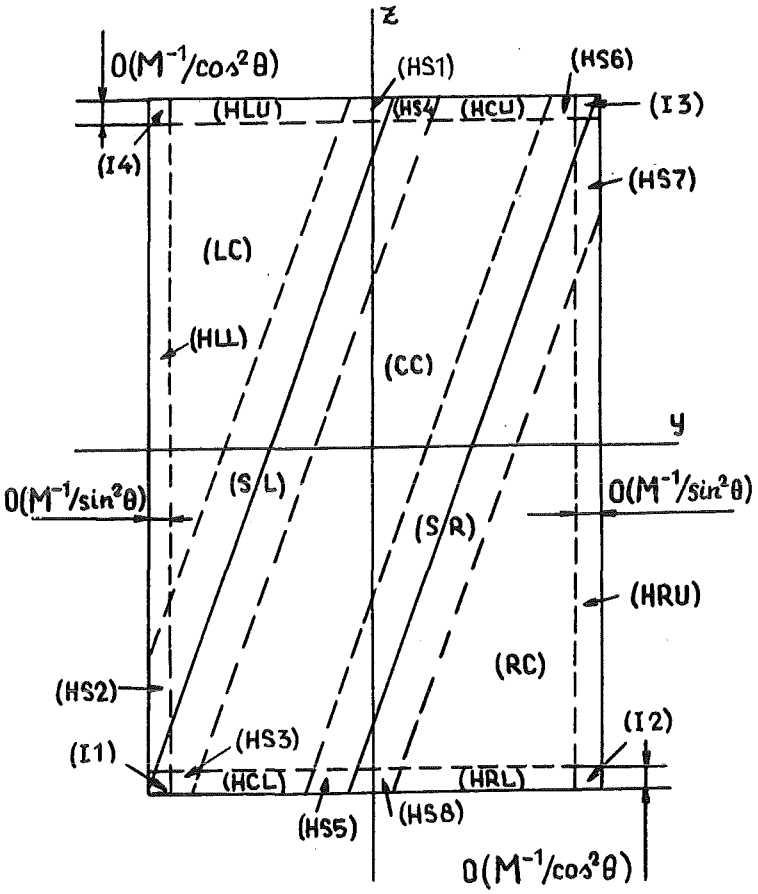

Fig. 2. 3 Flow subregions at high Hartmann number for $\tan\theta < l^{-1}$

2. 2. 1 Central core (region CC)

Considering the limit of equations (2.11) as $M \to \infty$ at fixed values of ξ and η one gets

$$\frac{\partial b_{CC}}{\partial \eta} = -\frac{k}{M'}, \qquad \frac{\partial v_{CC}}{\partial \eta} = 0. \tag{2.14}$$

Throughout § 2 the subscripts of variables v and b denote the region where corresponding limit equations are valid. The solution to the equations (2.14) is

$$v_{CC} = C_1(\xi), \qquad b_{CC} = -\eta\frac{k}{M} + C_2(\xi), \tag{2.15}$$

where $C_1(\xi)$ and $C_2(\xi)$ are arbitrary functions which are to be determined from the conditions of matching with the Hartmann-layer solutions (regions HCL, HCU).

2. 2. 2 Hartmann boundary layer HCU

Introducing boundary layer variables

$$\eta_1 = M\left[\eta - \xi\tan\theta - \frac{l}{\cos\theta}\right], \quad \xi_1 = \xi, \tag{2.16}$$

stretches the vicinity of the wall $z=l$. Substituting (2.16) into (2.11) in the limit $M \to \infty$ gives

$$\frac{\partial^2 v_{HCU}}{\partial\eta_1^2} + \cos^2\theta\frac{\partial b_{HCU}}{\partial\eta_1} = 0, \tag{2.17}$$

$$\frac{\partial^2 b_{HCU}}{\partial\eta_1^2} + \cos^2\theta\frac{\partial v_{HCU}}{\partial\eta_1} = 0. \tag{2.18}$$

The solutions to the equations (2.17), (2.18), which do not grow exponentially as $M \to \infty$ and satisfy the boundary conditions

$$v_{HCU} = 0, \quad b_{HCU} = 0 \qquad \text{at} \qquad \eta_1 = 0 \tag{2.19}$$

and conditions of matching with the functions v_{CC}, b_{CC} are

$$v_{HCU} = -b_{HCU} = C_1(\xi)\left[1 - \exp\left(\eta_1 \cos^2\theta\right)\right]. \tag{2.20}$$

The functions $C_1(\xi)$ and $C_2(\xi)$ are related by the expression

$$C_2(\xi) = \frac{k}{M}\left[\xi \tan\theta + \frac{l}{\cos\theta}\right] - C_1(\xi). \tag{2.21}$$

2. 2. 3 Hartmann boundary layer HCL

Introducing boundary layer variables

$$\eta_2 = M\left[\eta - \xi \tan\theta + \frac{l}{\cos\theta}\right], \quad \xi_2 = \xi, \tag{2.22}$$

stretches the vicinity of the wall $z=-l$. Substituting (2.22) into (2.11) in the limit $M \to \infty$ one gets the equations of the type (2.17), (2.18).

The solutions to these equations, which do not grow exponentially as $M \to \infty$ and satisfy the boundary conditions

$$v_{HCL} = 0, \quad b_{HCL} = 0 \qquad \text{at} \qquad \eta_2 = 0 \tag{2.23}$$

and conditions of matching with the functions v_{CC}, b_{CC} are

$$v_{HCL} = b_{HCL} = \frac{kl}{M\cos\theta}\left[1 - \exp\left(-\eta_2 \cos^2\theta\right)\right]. \tag{2.24}$$

The function $C_1(\xi)$ which is also determined from these conditions is

$$C_1(\xi) = \frac{kl}{M\cos\theta}. \tag{2.25}$$

Substituting (2.21), (2.25) into (2.15), (2.20) gives

$$v_{CC} = \frac{kl}{M\cos\theta}, \quad b_{CC} = \frac{k}{M}[-\eta + \xi\tan\theta], \tag{2.26}$$

$$v_{HCU} = -b_{HCU} = \frac{kl}{M\cos\theta}\left[1 - \exp\left(\eta_1\cos^2\theta\right)\right]. \tag{2.27}$$

Using the expressions (2.24), (2.26), (2.27) one can construct the composite expansions v_C, b_C, which are uniformly valid in regions CC, HCL, HCU (see Kevorkian & Cole, 1981)

$$v_C = \frac{kl}{M\cos\theta}\left[1 - \exp\left(\eta_1\cos^2\theta\right) - \exp\left(-\eta_2\cos^2\theta\right)\right], \tag{2.28}$$

$$b_C = \frac{k}{M}[-\eta + \xi\tan\theta] + \frac{kl}{M\cos\theta}\left[\exp\left(\eta_1\cos^2\theta\right) - \exp\left(-\eta_2\cos^2\theta\right)\right]. \tag{2.29}$$

2. 2. 4 Left core (region LC)

The equations governing the flow in the left core are of the form (2.14). The solution to these equations is

$$v_{LC} = C_3(\xi), \quad b_{LC} = -\frac{k}{M}\eta + C_4(\xi). \tag{2.30}$$

The arbitrary functions $C_3(\xi)$ and $C_4(\xi)$ are obtained from the conditions of matching with the solutions in the Hartmann layers HLU and HLL.

2. 2. 5 Hartmann boundary layer HLU

The functions v_{HLU} and b_{HLU} satisfy the equations (2.17), (2.18). The solution to these equations is obtained in the same way as in the section 2.2.2 for the functions v_{HCU} and b_{HCU}, so that

$$v_{HLU} = -b_{HLU} = C_3(\xi)\left[1 - \exp\left(\eta_1 \cos^2\theta\right)\right], \tag{2.31}$$

$$C_4(\xi) = -C_3(\xi) + \frac{k}{M}\left[\xi \tan\theta + \frac{1}{\cos\theta}\right]. \tag{2.32}$$

2. 2. 6 Hartmann boundary layer HLL

The boundary-layer variables

$$\eta_3 = M\left[\eta + \xi \cot\theta + \frac{1}{\sin\theta}\right], \quad \xi_3 = \xi \tag{2.33}$$

stretch the vicinity of the wall y=-1. Substituting (2.33) into (2.11) in the limit $M \to \infty$ gives

$$\frac{\partial^2 v_{HLL}}{\partial \eta_3^2} + \sin^2\theta \frac{\partial b_{HLL}}{\partial \eta_3} = 0, \tag{2.34}$$

$$\frac{\partial^2 b_{HLL}}{\partial \eta_3^2} + \sin^2\theta \frac{\partial v_{HLL}}{\partial \eta_3} = 0. \tag{2.35}$$

The solutions to the equations (2.34) and (2.35), which do not grow exponentially as $M \to \infty$ and satisfy the boundary conditions

$$v_{HLL} = 0, \quad b_{HLL} = 0 \qquad \text{at } \eta_3 = 0 \tag{2.36}$$

and the conditions of matching with the functions v_{LC}, b_{LC} are

$$v_{HLL} = b_{HLL} = C_3(\xi)\left[1 - \exp\left(-\eta_3 \sin^2\theta\right)\right]. \tag{2.37}$$

From these conditions the function $C_3(\xi)$ is also determined, so that

$$C_3(\xi) = \frac{k}{2M}\left[\xi(\tan\theta + \cot\theta) + \frac{1}{\sin\theta} + \frac{l}{\cos\theta}\right]. \tag{2.38}$$

The composite expansions v_L, b_L which are uniformly valid in the regions LC, HLU, HLL are

$$v_L = \frac{k}{2M}\left[\xi(\tan\theta + \cot\theta) + \frac{1}{\sin\theta} + \frac{l}{\cos\theta}\right]\times$$

$$\times\left\{1 - \exp\left(\eta_1 \cos^2\theta\right) - \exp\left(-\eta_3 \sin^2\theta\right)\right\}, \tag{2.39}$$

$$b_L = \frac{k}{2M}\left[\xi(\tan\theta + \cot\theta) + \frac{1}{\sin\theta} + \frac{l}{\cos\theta}\right]\times$$

$$\times\left\{-1 + \exp\left(\eta_1 \cos^2\theta\right) - \exp\left(-\eta_3 \sin^2\theta\right)\right\} -$$

$$-\frac{k}{M}\left[\eta - \xi\tan\theta - \frac{l}{\cos\theta}\right]. \tag{2.40}$$

From (2.26), (2.30), (2.32) and (2.38) follows that on the line $\xi = -\cos\theta + l\sin\theta$ which separates the left and the right cores the following relations hold

$$v_{CC} = v_{LC} = \frac{kl}{M\cos\theta}, \tag{2.41}$$

$$b_{CC} = b_{LC} = -\frac{k}{M}[\eta + \sin\theta - l\tan\theta\sin\theta], \tag{2.42}$$

i. e. the core velocity and induced magnetic field are continuous along this line. This means that the flow in the layer SL and adjacent Hartmann layers (HS1)-(HS4) are to be analysed only if higher-order approximations are of interest.

The solutions for the right core and adjacent Hartmann layers are obtained in analogous way.

2. 2. 7 Pressure gradient

The main term in the asymptotic expansion of the average velocity is

$$v_{av} = \frac{1}{4l}\int_{l\sin\theta-\cos\theta}^{\cos\theta-l\sin\theta} d\xi \int_{\xi\tan\theta-l/\cos\theta}^{\xi\tan\theta+l/\cos\theta} v_{CC}\,d\eta + \frac{1}{2l}\int_{-l\sin\theta-\cos\theta}^{l\sin\theta-\cos\theta} d\xi \int_{-\xi\cot\theta-1/\sin\theta}^{\xi\tan\theta+l/\cos\theta} v_{LC}\,d\eta =$$

$$= \frac{kl}{M\cos^2\theta}\left[\cos\theta - \frac{l}{3}\sin\theta\right]. \qquad (2.43)$$

Substituting (2.43) into (2.8) gives

$$k = \frac{M\cos\theta}{l\left[1-\frac{l}{3}\tan\theta\right]}. \qquad (2.44)$$

Since in the channel with insulating walls the layers SL and SR do not contribute to the main term of the asymptotics of the pressure gradient, the formula (2.44) is valid for $\theta \to 0$ as well.

Substituting (2.44) into (2.26), (2.30), (2.38) one gets

$$v_{CC} = \frac{1}{1-\frac{l}{3}\tan\theta}, \qquad (2.45)$$

$$v_{LC} = \frac{\cos\theta}{2l\left[1 - \frac{l}{3}\tan\theta\right]}\left[\xi(\tan\theta + \cot\theta) + \frac{1}{\sin\theta} + \frac{l}{\cos\theta}\right]. \qquad (2.46)$$

The results of calculations using formulas (2.45) and (2.46) are shown in figure 2.4.

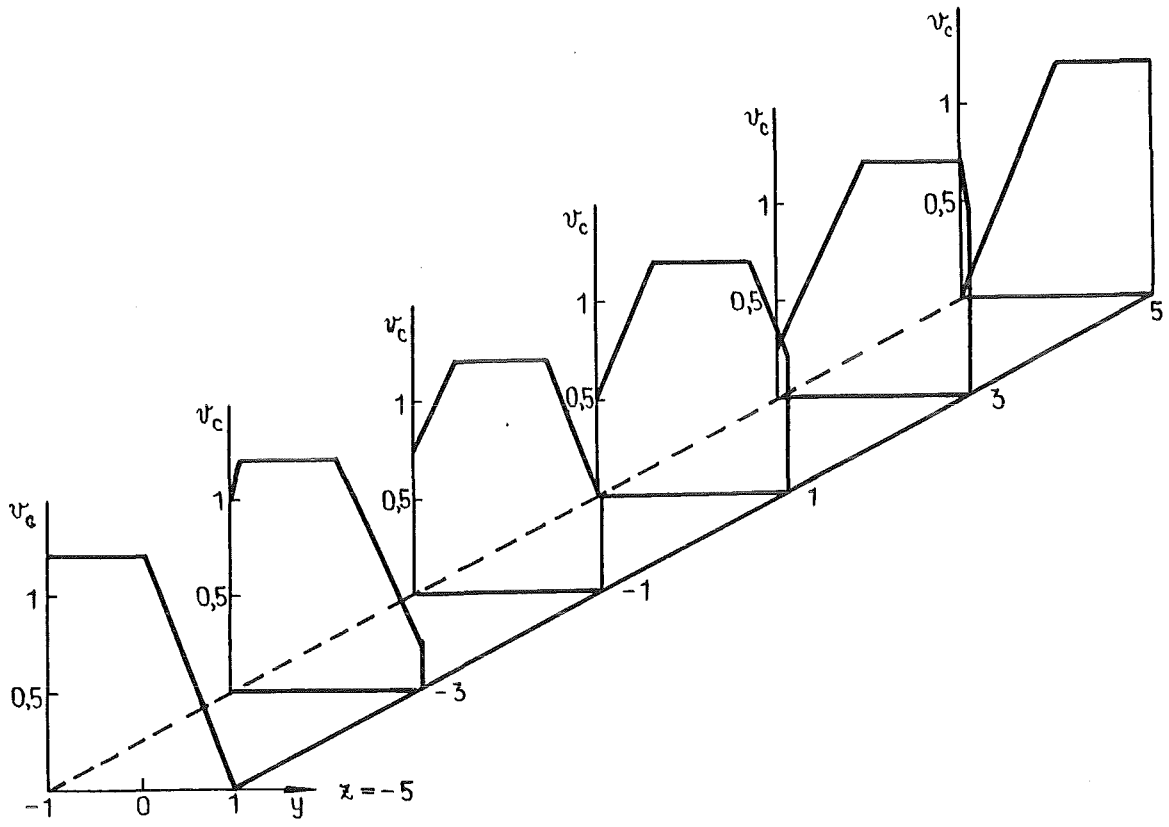

Fig. 2. 4 Core velocity for l=5 and $\tan\theta = 0.1$.

2. 3 Asymptotic solution for $\tan\theta = l^{-1}$

As $\tan\theta \to l^{-1}$ the layers SL and SR merge into a single layer S, and the central core disappears (figure 2.5). In the limit $\tan\theta \to l^{-1}$ the solution to the left core and adjacent

Hartmann layers and the formula (2.44) are still correct. Therefore in the case $\tan\theta = l^{-1}$ one can use the results of Sec. 2.2. Calculations with formula (2.46) are shown in figure 2.6.

2. 4 Asymptotic solution for $\tan\theta > l^{-1}$

In the case $\tan\theta > l^{-1}$ the layer S splits into two, and the central core reappears (see figure 2.7). However, in contrast to the case $\tan\theta < l^{-1}$ this core is between the walls $y = \pm 1$. The solutions for the left core and adjacent Hartmann layers with undetermined k obtained in Sec. 2.2 are still valid. The solutions for the central core and adjacent Hartmann layers are obtained in the same way. Therefore we present only the final results

$$v_{CC} = \frac{l}{l - \frac{1}{3}\cot\theta}, \tag{2.47}$$

$$b_{CC} = -\frac{l\sin\theta}{l - \frac{1}{3}\cot\theta}\left[\eta + \xi\cot\theta\right], \tag{2.48}$$

$$v_{LC} = \frac{l\sin\theta}{2\left[l - \frac{1}{3}\cot\theta\right]}\left[\xi(\tan\theta + \cot\theta) + \frac{1}{\sin\theta} + \frac{l}{\cos\theta}\right], \tag{2.49}$$

$$b_{LC} = \frac{l\sin\theta}{2\left[l - \frac{1}{3}\cot\theta\right]}\left[\xi(\tan\theta - \cot\theta) - 2\eta - \frac{1}{\sin\theta} + \frac{l}{\cos\theta}\right], \tag{2.50}$$

$$k = \frac{Ml\sin\theta}{l - \frac{1}{3}\cot\theta}. \tag{2.51}$$

Variation of the pressure gradient with θ for different values of l is shown in figure 2.8. Calculations are done using combination of formulas (2.44) and (2.51) which covers the range $0^o \le \theta \le 90^o$.

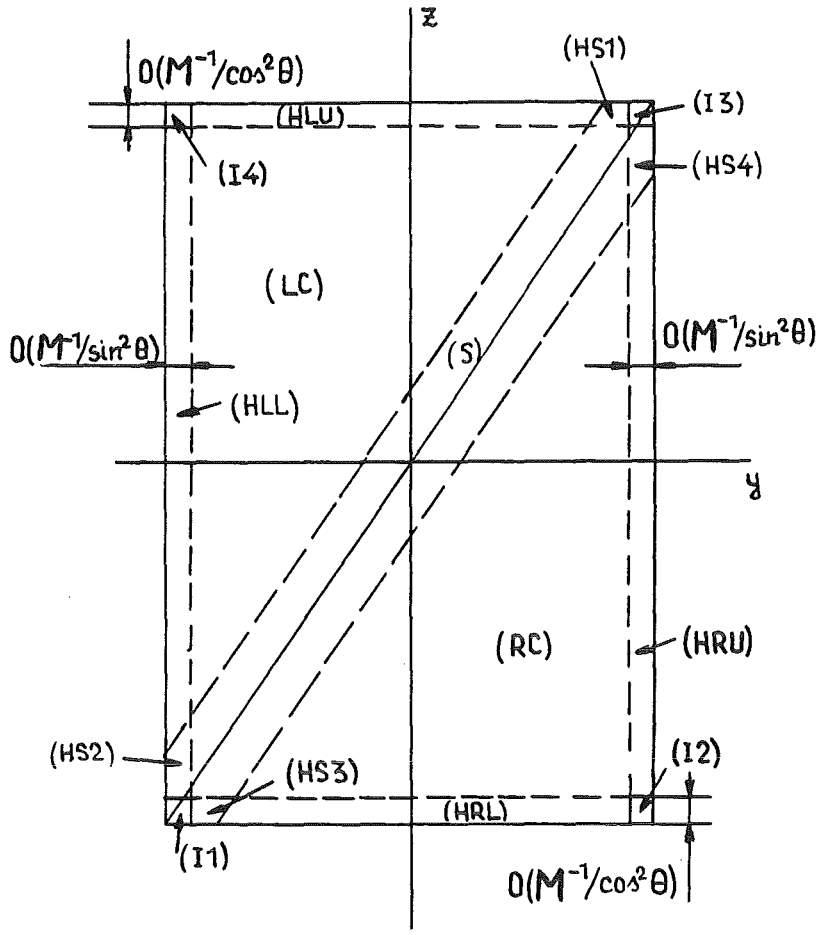

Fig. 2. 5 Flow subregions at high Hartmann number for $\tan\theta = l^{-1}$

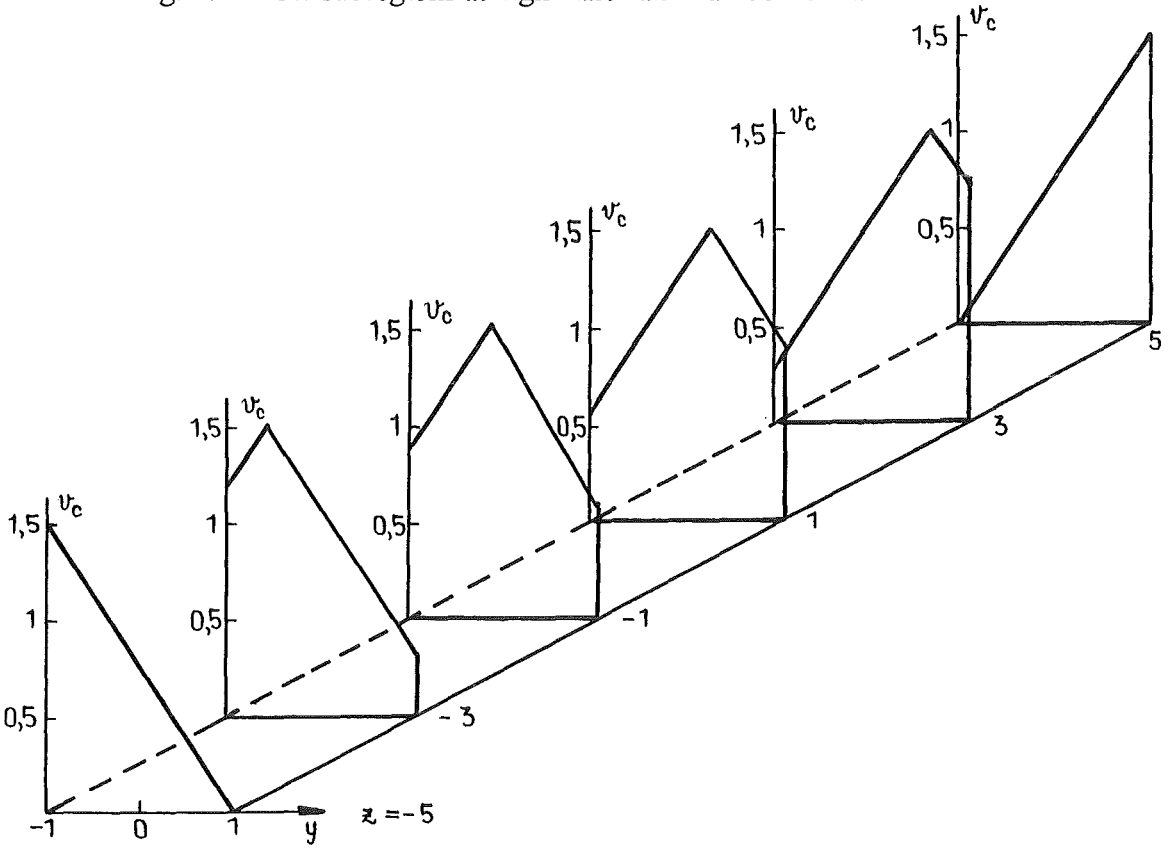

Fig. 2. 6 Core velocity for $l=5$ and $\tan\theta = 0.2$.

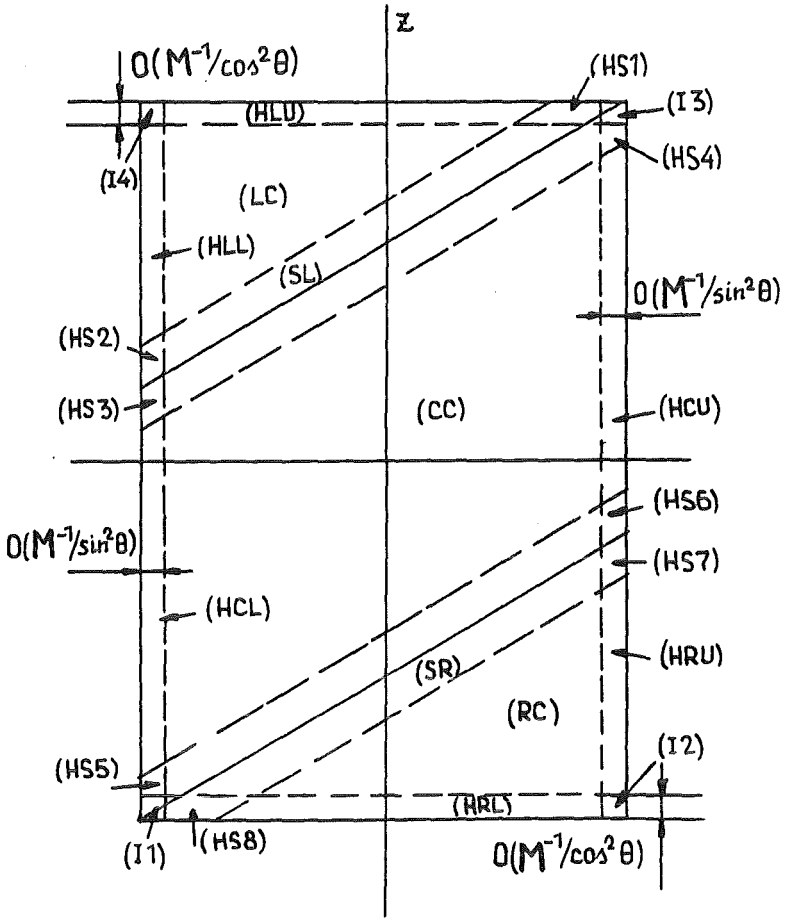

Fig. 2. 7 Flow subregions at high Hartmann number for tan $\theta > l^{-1}$

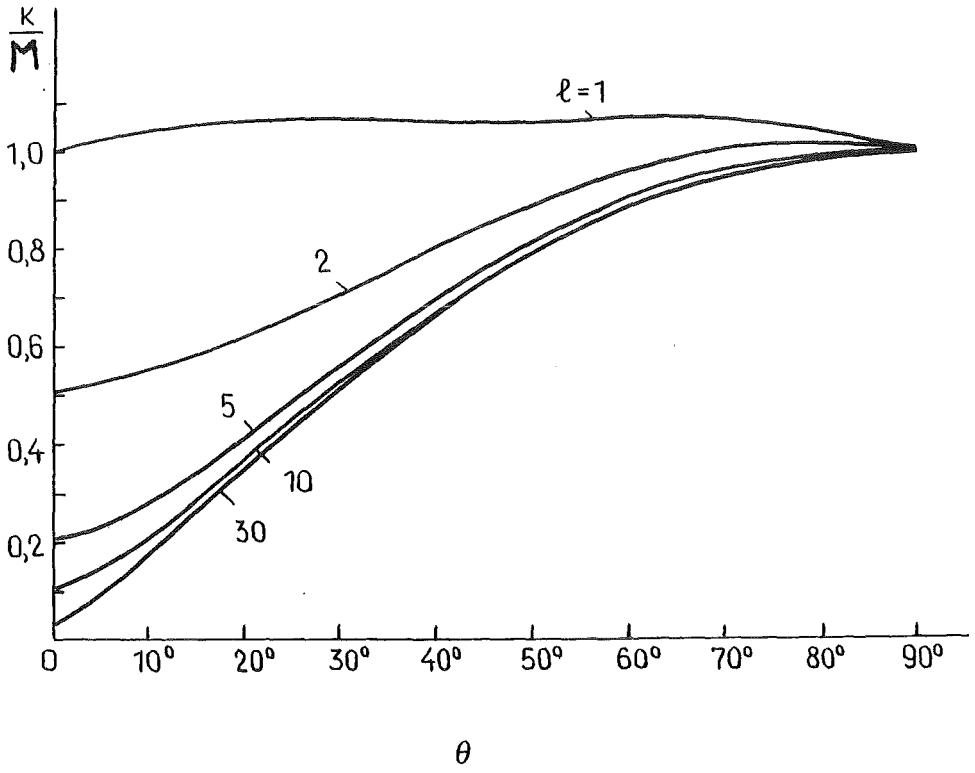

Fig. 2. 8 Variation of the normalised pressure gradient with θ for different values of l.

3. Fully developed MHD flows in slotted channels

3. 1 Basic equations and boundary conditions

Consider the steady flow of a viscous, electrically conducting (σ=*const)*, incompressible fluid in a rectangular channel $|x| < \infty, |y| < a/2, |z| < h/2$ driven by the pressure gradient *dp/dx=const* in a uniform, constant magnetic field $\underline{B}_0 = \{0, 0, B_0\}$. In this case the fluid velocity $\underline{v} = v(y,z)\underline{e}_x$ and the induced electric current

$$j_y(y,z) = \frac{1}{\mu_0}\frac{\partial B_{i,x}}{\partial z}, \qquad j_z(y,z) = -\frac{1}{\mu_0}\frac{\partial B_{i,x}}{\partial y}$$

depend on the transverse co-ordinates only and are determined from the equations, which in the dimensionless form reads (e. g. Shercliff, 1965)

$$\nabla^2 v + M\frac{\partial b}{\partial z} = P, \qquad \nabla^2 b + M\frac{\partial v}{\partial z} = 0, \tag{3.1}$$

where $M = B_0 a\sqrt{\frac{\sigma}{\rho\nu}}$ is the Hartmann number, and $P = \frac{a^2}{\rho\nu v_0}\frac{dp}{dx}$ is the dimensionless pressure gradient. The characteristic length a is the width of the channel, the characteristic velocity is v_0, and the characteristic value of the induced magnetic field $\left(B_{i,x} = bB_i^*\right)$ is $B_i^* = v_0\mu_0\sqrt{\sigma\rho\nu}$. The flow geometry in the dimensionless form is shown in figure 3.1.

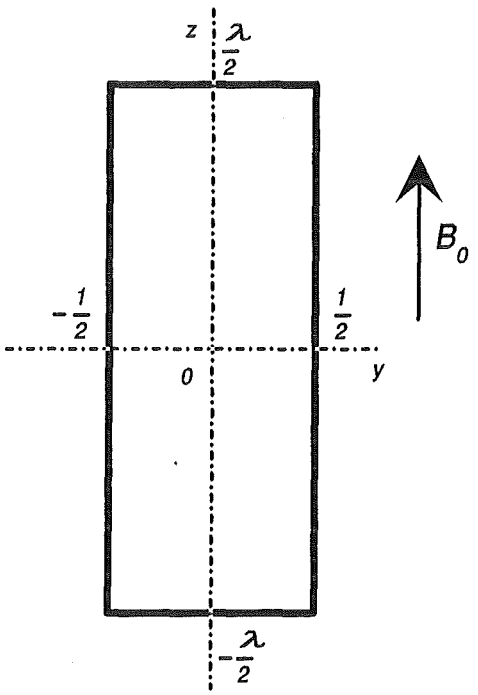

Fig. 3.1 Schematic diagram of flow in a slotted channel.

The system of equations (3.1) is to be solved under the following boundary conditions.

1. Non-slip conditions

$$v(\pm 1/2, z) = v(y, \pm \lambda/2) = 0, \quad \lambda = h / a. \tag{3.2}$$

2. The boundary conditions for the induced magnetic field $b(y,z)$ are determined by the electrical properties of the channel walls. If, for simplicity, one assumes that "linear conductivities", i.e. the values $\sigma_{wi}h_{wi}$, for opposite channel walls are equal, and the electrically conducting wall is thin, then these conditions can be written as follows (Shercliff, 1956)

   - at the side walls $y = \pm\frac{1}{2}$, parallel to the external field
   $$b \pm c_2 \frac{\partial b}{\partial y} = 0, \quad c_2 = \frac{\sigma_{w2}h_{w2}}{\sigma a}, \tag{3.3}$$
   - at the Hartmann walls $z = \pm\lambda / 2$
   $$b \pm c_1 \frac{\partial b}{\partial y} = 0, \quad c_1 = \frac{\sigma_{w1}h_{w1}}{\sigma a}. \tag{3.4}$$

3. Consider now the boundary conditions in the case when an infinitely thin layer with a finite Ohmic resistance separates the electrically conducting wall from the liquid metal. Such a contact resistance may exist when the working fluid is Pb-Bi, for example, which creates a stable oxide film on channel walls.

For simplicity, in the first approximation, the electric properties of this film are assumed to be constant, so that the jump of the electric potential across the layer is directly proportional to the electric current. While deriving the boundary conditions the following model has been used (see figure 3.2). Imagine that there is a stagnant layer of width h_k between the liquid metal and the wall having anisotrophic conductivity $\hat{\sigma}_k$, so that in the direction perpendicular to the wall its conductivity is equal to σ_k, and in the direction parallel to the wall - to zero. It is clear, of course, that both the wall thickness h_w and h_k are much smaller than the radius of curvature of the wall surface.

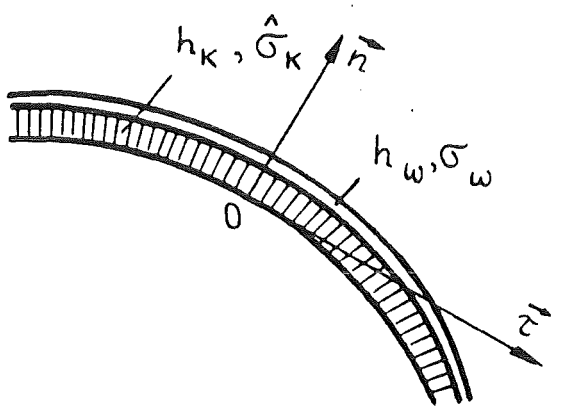

Fig. 3. 2 Schematic diagram of an electrically conducting wall covered by an insulating coating

Since the electric currents in the channel are two-dimensional, the electric potential ϕ^w and the induced magnetic field B_i^w in the wall $(h_k \le n < h_k + h_w)$ are related by the expressions

$$\frac{1}{\mu_0}\frac{\partial B_i^w}{\partial n} = -\sigma_w \frac{\partial \phi^w}{\partial \tau}, \qquad \frac{1}{\mu_0}\frac{\partial B_i^w}{\partial \tau} = \sigma_w \frac{\partial \phi^w}{\partial n}. \tag{3.5}$$

Integrating the first equation in (3.5) across the wall and using the fact that B_i^w is equal to zero at the outer wall surface gives

$$\frac{1}{\mu_0} B_i^w(\tau, h_k) = \sigma_w \frac{\partial}{\partial \tau} \int_{h_k}^{h_k+h_w} \phi^w(\tau, n) dn. \tag{3.6}$$

The value $\phi^w(\tau, n)$ can be represented by the Taylor series expansion, which, taking into account the condition $\frac{\partial \phi^w}{\partial n}(\tau, h_k + h_w) = 0$, reads

$$\phi^w(\tau, n) = \phi^w(\tau, h_k) + \tfrac{1}{2}\frac{\partial^2 \phi^w}{\partial n^2}(\tau, h_k)\left[(n-h_k)^2 - 2h_w(n-h_k)\right] + \dots . \tag{3.7}$$

Substituting (3.7) into (3.6) and integrating the resulting equation one gets

$$\frac{1}{\mu_0} B_i^w(\tau, h_k) = \sigma_w h_w \frac{\partial}{\partial \tau}\left\{\phi^w(\tau, h_k) - \frac{h_w^2}{3}\frac{\partial^2 \phi^w}{\partial n^2}(\tau, h_k) + \dots\right\}.$$

Using further the thin-wall approximation which assumes that $h_w << 1$ gives

$$\frac{1}{\mu_0} B_i^w(\tau, h_k) = \sigma_w h_w \frac{\partial \phi^w}{\partial \tau}(\tau, h_k). \tag{3.8}$$

At the same time for the intermediate contact layer $(0 \le n \le h_k)$ the following expressions hold

$$\frac{1}{\mu_0}\frac{\partial B_i^k}{\partial n} = 0, \qquad \frac{1}{\mu_0}\frac{\partial B_i^k}{\partial \tau} = \sigma_k \frac{\partial \phi^k}{\partial n}. \tag{3.9}$$

From the first equation in (3.9) it follows that the function $B_i^k(\tau, n)$ is independent of the normal co-ordinate n, so that $B_i^k(\tau, 0) = B_i^k(\tau, h_k)$. Therefore, by integrating the second equation in (3.9) across the contact layer one gets

$$\phi^k(\tau, h_k) - \phi^k(\tau, 0) = \frac{h_k}{\mu_0 \sigma_k} \frac{\partial B_i^*}{\partial \tau}(\tau, 0).$$

Using continuity of both the electric potential and the magnetic field at the boundaries $n=0$ and $n = h_k$ gives

$$-\frac{\partial \phi}{\partial \tau}(\tau, 0) + \frac{\partial \phi}{\partial \tau}(\tau, h_k) - \frac{h_k}{\mu_0 \sigma_k} \frac{\partial^2 B_i}{\partial \tau^2}(\tau, 0) = 0.$$

From (3.8) follows that $\frac{\partial \phi^w}{\partial \tau}(\tau, h_k) = \frac{1}{\mu_0 \sigma_w h_w} B_i(\tau, 0)$. The value $\frac{\partial \phi}{\partial \tau}(\tau, 0)$ can also be expressed in terms of the magnetic field B_i, taking into account the non-slip condition on the boundary. The result is

$$\frac{\partial \phi}{\partial \tau}(\tau, 0) = -\frac{1}{\mu_0 \sigma} \frac{\partial B_i}{\partial n}(\tau, 0),$$

so that

$$\frac{1}{\sigma} \frac{\partial B_i}{\partial n}(\tau, 0) + \frac{1}{\sigma_w h_w} B_i(\tau, 0) - \frac{h_k}{\sigma_k} \frac{\partial^2 B_i}{\partial \tau^2}(\tau, 0) = 0.$$

The last boundary condition may be rewritten in the dimensionless form, namely

$$b + c \frac{\partial b}{\partial n} - cr \frac{\partial^2 b}{\partial \tau^2} = 0, \qquad (3.10)$$

where $c = \frac{\sigma_w h_w}{\sigma a}$, $r = \frac{\sigma h_k}{\sigma_k a}$. The ratio h_k / σ_k which appears in the parameter r can be interpreted as the specific contact electrical resistance R_k, so that

$$r = R_k \frac{\sigma}{a}.$$

It is evident that for $r=0$ the equation (3.10) becomes the usual thin-wall boundary condition, such as (3.3) and (3.4). For $r \to \infty$ and finite value of c from (3.10) follows the condition on the insulating wall, namely $\partial b / \partial \tau = 0$.

3. 2 Semi-infinite slotted channel ($\lambda \to \infty$)

In this section the results for the flow of an electrically conducting medium in a semi-infinite MHD-channel $(|x| < \infty, |y| < 1/2, z > 0)$ are presented. For convenience the coordinate system is shifted in the z-direction by -1/2 and then the limit $\lambda \to \infty$ is considered. The geometry is shown in figure 3.3.

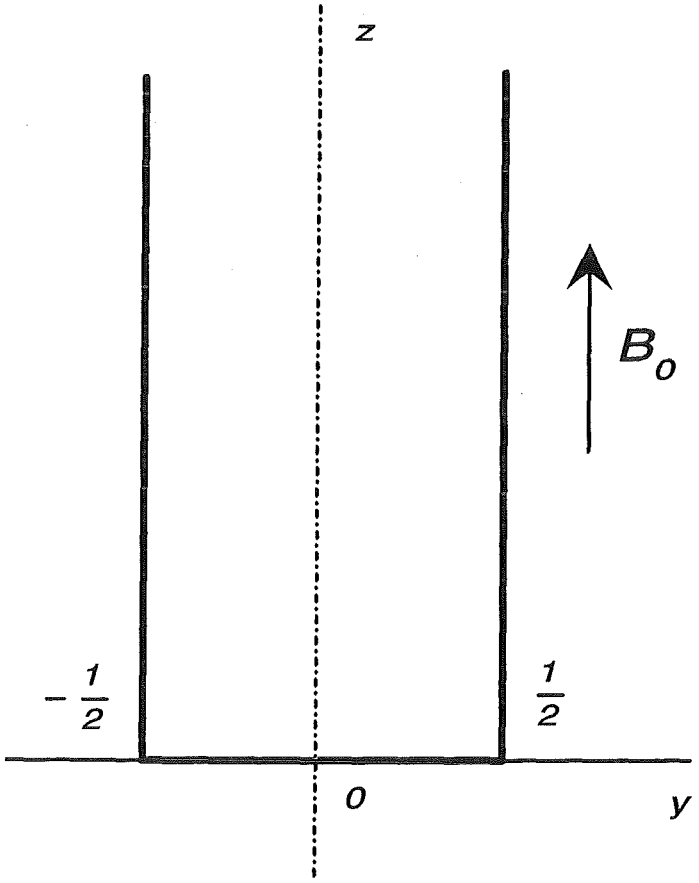

Fig. 3.3 Schematic diagram of flow in a semi-infinite channel.

It is convenient to choose the value

$$v_0 = -\frac{a}{8\rho\nu}\frac{dp}{dx}$$

as the characteristic velocity, which is proportional to the applied pressure gradient. Then the system (3.1) can be written as follows

$$\nabla^2 v + M\frac{\partial b}{\partial z} = -8, \qquad \nabla^2 b + M\frac{\partial v}{\partial z} = 0. \tag{3.11}$$

Such a choice of v_0 leads to the following expression for the non-dimensional velocity

$$v(y,\infty) = 1 - 4y^2 \qquad \text{as } z \to \infty$$

in the region where the MHD-interaction vanishes and the flow is of Poisseuille type.

Consider the simplest case when the walls at $y = \pm\frac{1}{2}$ parallel to the external magnetic field are insulating $\left(c_{\parallel} = 0\right)$. The boundary condition for the electrical variables at the wall $z=0$ is determined by the expression (3.10), which reads

$$b - c_{\perp}\frac{\partial b}{\partial z} - c_{\perp} r\frac{\partial^2 b}{\partial y^2} = 0.$$

The solution to this boundary-value problem can be easily obtained in terms of trigonometric series with basic functions $\cos \alpha_k y$, where

$$\alpha_k = \pi(2k - 1), \qquad k = 1, 2, 3, \ldots.$$

As a result one gets

$$v(y,z) = 1 - 4y^2 + \sum_{k=1}^{\infty} \left\{ A_k \exp\left[-\left(\nu_k + \frac{M}{2} \right) z \right] + B_k \exp\left[-\left(\nu_k - \frac{M}{2} \right) z \right] \right\} \cos \alpha_k y,$$

$$b(y,z) = \sum_{k=1}^{\infty} \left\{ A_k \exp\left[-\left(\nu_k + \frac{M}{2} \right) z \right] - B_k \exp\left[-\left(\nu_k - \frac{M}{2} \right) z \right] \right\} \cos \alpha_k y, \qquad (3.12)$$

where

$$A_k = \frac{16(-1)^k}{\alpha_k^3} \frac{1 + c_\perp \left(\nu_k - \frac{M}{2} \right) + c_\perp r \alpha_k^2}{1 + c_\perp \nu_k + c_\perp r \alpha_k^2},$$

$$B_k = \frac{16(-1)^k}{\alpha_k^3} \frac{1 + c_\perp \left(\nu_k + \frac{M}{2} \right) + c_\perp r \alpha_k^2}{1 + c_\perp \nu_k + c_\perp r \alpha_k^2},$$

$$\nu_k = \sqrt{\alpha_k^2 + M^2/2}.$$

From the solution obtained it follows that the length of the region in the z-direction, where the moving medium interacts with the magnetic field, is proportional to M and is almost independent of the electrical properties of the Hartmann wall. This is illustrated in figures 3.4 and 3.5, which show velocity distribution at the channel axis $y=0$. The velocity profiles $v(0,z)$, calculated with formula (3.12) for certain values of parameter M, are shown in figure 3.4 for the case when the electric currents do not shortcut in the wall ($c_\perp = 0$ or $r = \infty$). Note that for $M \geq 100$ the velocity profiles become practically self-modeling with respect to the parameter z/M.

The dependence of the velocity distribution on the value of the wall conductance ratio $c_\perp$ for $r=0$ and $M=100$ is shown in figure 3.5. It is seen that with increasing $c_\perp$ the values of the velocity at the outer boundary of the Hartmann layer decrease, and for $c_\perp \to \infty$ this layer almost disappears. Figure 3.6 shows velocity distribution $v(y)$ against the channel width for the

case $c_\perp = \infty$ at different distances from the Hartmann wall. This velocity distribution at any cross-section of the semi-infinite channel and for arbitrary values of parameters M, $c_\perp$ and r has non-monotonic nature, i.e. it has the maximum value at the channel axis and vanishes at the channel walls.

In conclusion we should mention that the results obtained for the semi-infinite channel are of practical importance only if the parameter M does not exceed the aspect ratio $\lambda = h / a$ of the actual channel. In reality, usually, opposite is true.

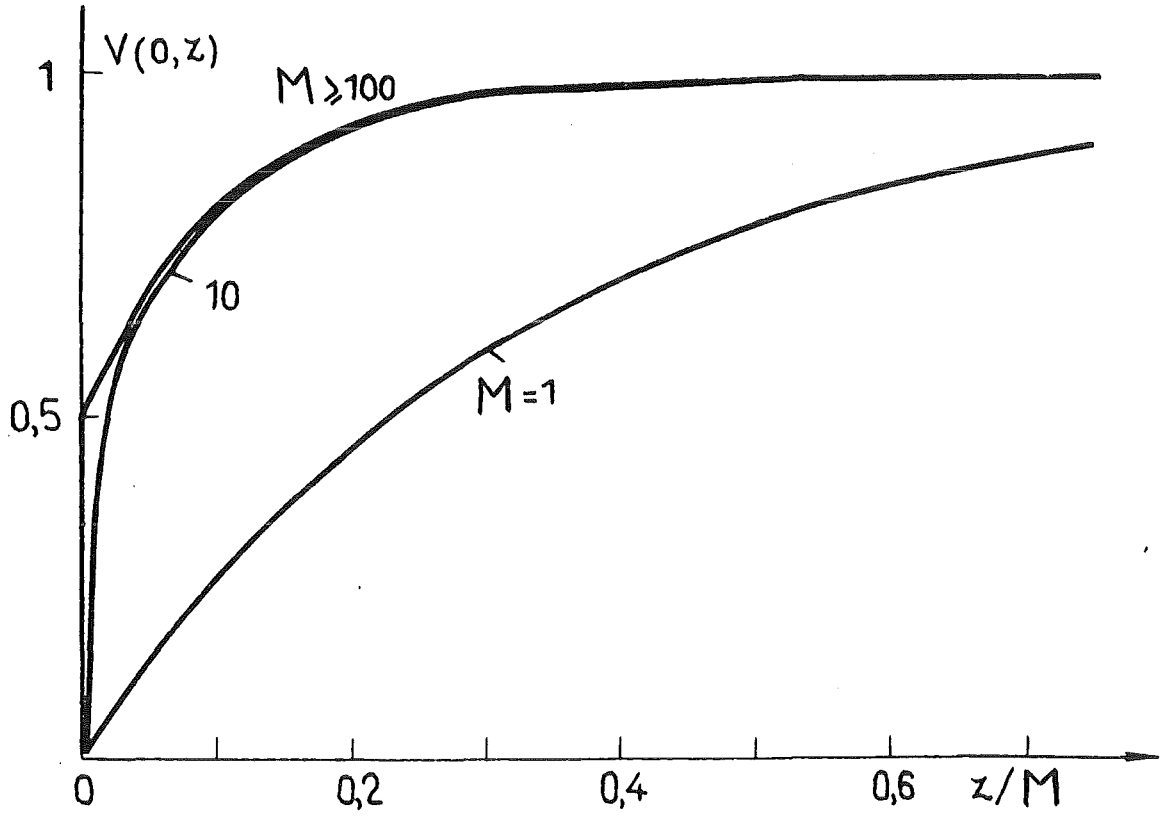

Fig. 3.4 Fluid velocity in a semi-infinite channel at the channel axis y=0 for different values of the Hartmann number.

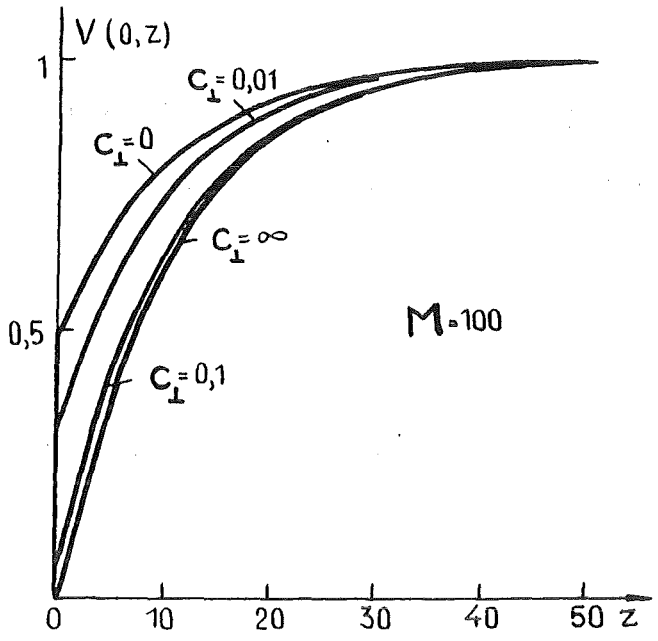

Fig. 3.5 Fluid velocity in a semi-infinite channel at the channel axis y=0 for different values of the wall conductance ratio.

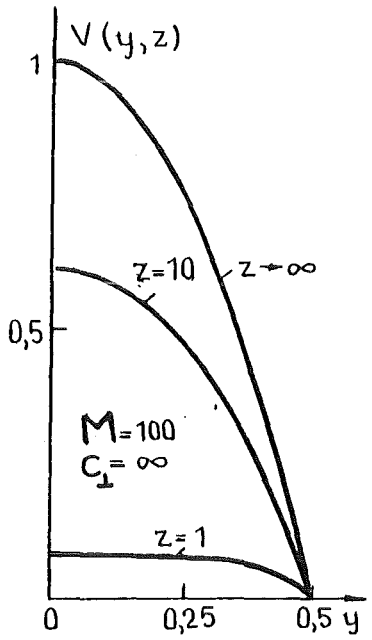

Fig. 3. 6 Fluid velocity in a semi-infinite channel for different values of z.

3. 3 MHD flow in a slotted channel with insulating coating

As was mentioned above (§ 3.1), the distributions of hydrodynamic and electrodynamic fields in a slotted channel are described by the system of equations

$$\nabla^2 v + M\frac{\partial b}{\partial z} = P, \qquad \nabla^2 b + M\frac{\partial v}{\partial z} = 0. \tag{3.13}$$

This system will be solved together with the following boundary conditions:

- the non-slip conditions

$$v(\pm 1/2, z) = v(y, \pm\lambda/2) = 0, \tag{3.13a}$$

- if walls parallel to the external magnetic field are insulating $\left(c_{\parallel} = 0\right)$ one gets

$$b(\pm 1/2, z) = 0, \tag{3.13b}$$

- the electrical boundary condition with contact resistance (or insulating coating)

$$b \pm c_1\frac{\partial b}{\partial z} - c_1 r\frac{\partial^2 b}{\partial y^2} = 0 \qquad \text{at } z = \pm\lambda/2. \tag{3.13c}$$

Choosing average velocity v_{av} as the characteristic velocity v_0 one gets the following expression

$$\frac{1}{\lambda}\int_{-1/2}^{1/2} dy \int_{-\lambda/2}^{\lambda/2} v(y,z)dz = 1. \tag{3.13d}$$

The last condition allows to determine the pressure gradient dp / dx uniquely. Indeed, from the structure of the boundary value problem (3.13) it follows that its solution has the form

$$v(y,z) = Pv_1(M,y,z), \quad b(y,z) = Pb_1(M,y,z).$$

The functions v_1 and b_1 do not depend on the parameter $P = \dfrac{a}{\rho\nu v_0}\dfrac{dp}{dx}$. Hence from the condition (3.13d) one gets

$$P(M,\lambda,c_1,r) = \left\{\frac{1}{\lambda}\int_{-1/2}^{1/2} dy \int_{-\lambda/2}^{\lambda/2} v_1(M,y,z)dz\right\}^{-1}, \tag{3.14}$$

$$\frac{dp}{dx} = \frac{\rho\nu}{a} v_0 P(M,\lambda,c_1,r). \tag{3.15}$$

The solution of the problem (3.13) is

$$v(y,z) = 4P\sum_{k=1}^{\infty}(-1)^k \frac{\cos\alpha_k y}{\alpha_k^3}\left\{1 - A_k\frac{\cosh\left(\nu_k+\frac{M}{2}\right)z}{\cosh\left(\nu_k+\frac{M}{2}\right)\frac{\lambda}{2}} - B_k\frac{\cosh\left(\nu_k-\frac{M}{2}\right)z}{\cosh\left(\nu_k-\frac{M}{2}\right)\frac{\lambda}{2}}\right\}, \tag{3.16}$$

$$b(y,z) = 4P\sum_{k=1}^{\infty}(-1)^k \frac{\cos\alpha_k y}{\alpha_k^3}\left\{A_k\frac{\sinh\left(\nu_k+\frac{M}{2}\right)z}{\cosh\left(\nu_k+\frac{M}{2}\right)\frac{\lambda}{2}} - B_k\frac{\sinh\left(\nu_k-\frac{M}{2}\right)z}{\cosh\left(\nu_k-\frac{M}{2}\right)\frac{\lambda}{2}}\right\},$$

where

$$A_k = \frac{c_1\left(\nu_k-\frac{M}{2}\right) + \left(1+c_1 r\alpha_k^2\right)\tanh\left(\nu_k-\frac{M}{2}\right)\frac{\lambda}{2}}{2c_1\nu_k + \left(1+c_1 r\alpha_k^2\right)\left[\tanh\left(\nu_k+\frac{M}{2}\right)\frac{\lambda}{2} + \tanh\left(\nu_k-\frac{M}{2}\right)\frac{\lambda}{2}\right]},$$

$$B_k = \frac{c_1\left(\nu_k + \frac{M}{2}\right) + \left(1 + c_1 r\alpha_k^2\right)\tanh\left(\nu_k + \frac{M}{2}\right)\frac{\lambda}{2}}{2c_1\nu_k + \left(1 + c_1 r\alpha_k^2\right)\left[\tanh\left(\nu_k + \frac{M}{2}\right)\frac{\lambda}{2} + \tanh\left(\nu_k - \frac{M}{2}\right)\frac{\lambda}{2}\right]},$$

$$\nu_k = \sqrt{\alpha_k^2 + M^2/2}, \qquad \alpha_k = \pi(2k - 1),$$

while the value of P, according to (3.14), is

$$P(M,\lambda,c_1,r) = -\left\{8\sum_{k=1}^{\infty}\frac{1}{\alpha_k^4}\left[1 - A_k\frac{\tanh\left(\nu_k + \frac{M}{2}\right)\frac{\lambda}{2}}{\left(\nu_k + \frac{M}{2}\right)\frac{\lambda}{2}} - B_k\frac{\tanh\left(\nu_k - \frac{M}{2}\right)\frac{\lambda}{2}}{\left(\nu_k - \frac{M}{2}\right)\frac{\lambda}{2}}\right]\right\}^{-1}. \qquad (3.17)$$

If the magnetic field is absent *(M=0)*, the velocity distribution in the channel and the value of P are, of course, independent of electrical properties of the walls but depend on the aspect ratio λ. In this case from the formulas (3.16) follows

$$v(y,z) = 4P(0,\lambda)\sum_{k=1}^{\infty}(-1)^k\frac{\cos\alpha_k y}{\alpha_k^3}\left\{1 - \frac{\cosh\alpha_k z}{\cosh\frac{\alpha_k\lambda}{2}}\right\}, \qquad (3.18)$$

$$P(0,\lambda) = -\left\{8\sum_{k=1}^{\infty}\frac{1}{\alpha_k^4}\left[1 - \frac{2\tanh\frac{\alpha_k\lambda}{2}}{\alpha_k\lambda}\right]\right\}^{-1}. \qquad (3.18a)$$

In the table below certain values of function $P(0,\lambda)$ are presented.

λ	1	5	10	15	20	25	30	50	∞
$P(0,\lambda)$	28.4	13.73	12.8	12.5	12.38	12.32	12.25	12.16	12

The effect of the magnetic field and the electrical properties of the walls on the integral channel properties can be evaluated by the quantity

$$\Lambda(M,\lambda,c_1,r)=\frac{P(M,\lambda,c_1,r)}{P(0,\lambda)}, \tag{3.19}$$

which shows the increase of the pressure gradient due to MHD phenomena. The formula for Λ is

$$\Lambda=\frac{\displaystyle\sum_{k=1}^{\infty}\frac{1}{\alpha_k^4}\left[1-\frac{2\tanh\dfrac{\alpha_k\lambda}{2}}{\alpha_k\lambda}\right]}{\displaystyle\sum_{k=1}^{\infty}\frac{1}{\alpha_k^4}\left[1-A_k\frac{\tanh\left(\nu_k+\dfrac{M}{2}\right)\dfrac{\lambda}{2}}{\left(\nu_k+\dfrac{M}{2}\right)\dfrac{\lambda}{2}}-B_k\frac{\tanh\left(\nu_k-\dfrac{M}{2}\right)\dfrac{\lambda}{2}}{\left(\nu_k-\dfrac{M}{2}\right)\dfrac{\lambda}{2}}\right]}. \tag{3.19a}$$

The values of $\Lambda(M,\lambda,c_1,r)$, calculated from (3.19a) are shown in Appendix A.

The dimensional pressure gradient can be calculated from the expression

$$\frac{dp}{dx}=\frac{\rho\nu}{S}v_{av}\lambda P(0,\lambda)\Lambda(M,\lambda,c_1,r), \tag{3.20}$$

where $S=ah$ is the area of the channel cross-section. From this expression one gets the hydraulic power per unit length, namely

$$P_{HYD}=\Delta pQ=\rho\nu\lambda v_{av}^2P(0,\lambda)\Lambda(M,\lambda,c_1,r). \tag{3.21}$$

Note that the geometrical size of the channel does not enter the formula (3.21), but at the same time it determines the values of the parameters M, c_1 and r. In addition the following relation holds

$$\lambda P(0,\lambda)=\frac{1}{\lambda}P\left(0,\frac{1}{\lambda}\right).$$

Consider the dependence of the integral flow quantities on the aspect ratio λ at fixed cross-sectional area. For simplicity we consider the case when the channel walls are insulating $(c_1 = 0)$. Then, at high values of M $\left(\lambda M >> 1, \sqrt{M/2\lambda} >> 1\right)$, the expression for $\Lambda(M, \lambda, 0, 0)$ is approximated by the following formula with high order of accuracy, see Vatazhin, Liubimov & Regirer, 1970 (this can be checked by using the exact values from the table in Appendix A)

$$\Lambda = \frac{2M}{\lambda P(0,\lambda)\left(1 - \frac{2}{\lambda M} - \frac{0,852}{\sqrt{M/2\lambda}}\right)}. \tag{3.22}$$

Since $S=ah=const$, then $a = \sqrt{S/\lambda}$ and

$$M = aB_0\sqrt{\frac{\sigma}{\rho\nu}} = B_0\sqrt{\frac{S\sigma}{\lambda\rho\nu}} \cong \frac{1}{\sqrt{\lambda}},$$

so that the value of the pressure gradient (and pressure losses) in the first approximation is inversely proportional to $\sqrt{\lambda}$, i. e. it decreases with increasing aspect ratio. It is clear that the presence of the electrically conducting walls may only strengthen this tendency.

Consider now the local flow quantities. The distribution of velocity $v(0,z)$ on the axis $y=0$ of the slotted channel with insulating walls $(\lambda = 20, c_1 = 0)$ is shown in figure 3.7. It is seen that with increasing Hartmann number the Hartmann layer is formed at the walls perpendicular to the magnetic field, and the velocity profile, starting from certain considerably high values of M becomes more and more uniform, and $v(0,z) \to 1$ as $M \to \infty$. At high values of M (such that $\sqrt{M/2\lambda} >> 1$) the velocity distribution in such a channel with insulating walls can be approximated by the following expression

$$v(y,z) = \frac{\left\{1 - \frac{\cosh\left(\sqrt{\frac{M}{2\lambda}}\frac{2y}{0.852}\right)}{\cosh\left(\sqrt{\frac{M}{2\lambda}}\frac{1}{0.852}\right)}\right\}\left\{1 - \frac{\cosh Mz}{\cosh\frac{M\lambda}{2}}\right\}}{1 - \frac{2}{\lambda M} - 0.852\sqrt{\frac{2\lambda}{M}}}. \tag{3.22a}$$

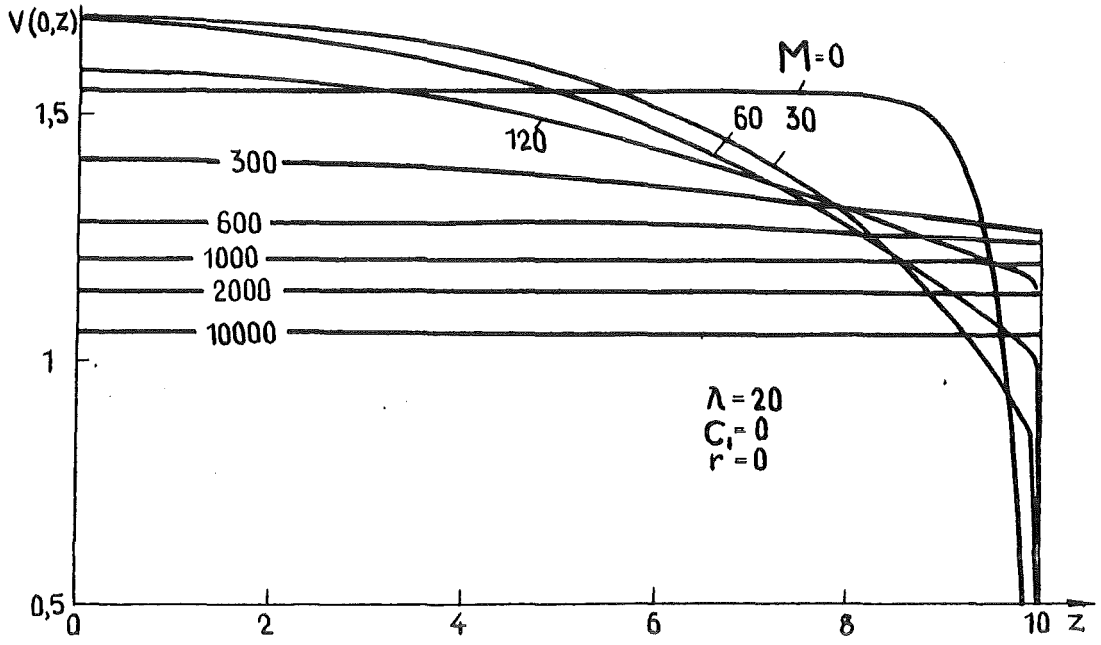

Fig. 3.7 Fluid velocity in a rectangular slotted channel at the channel axis $y=0$ for different values of the Hartmann number. The Hartmann wall is insulating $(c_1 = 0)$.

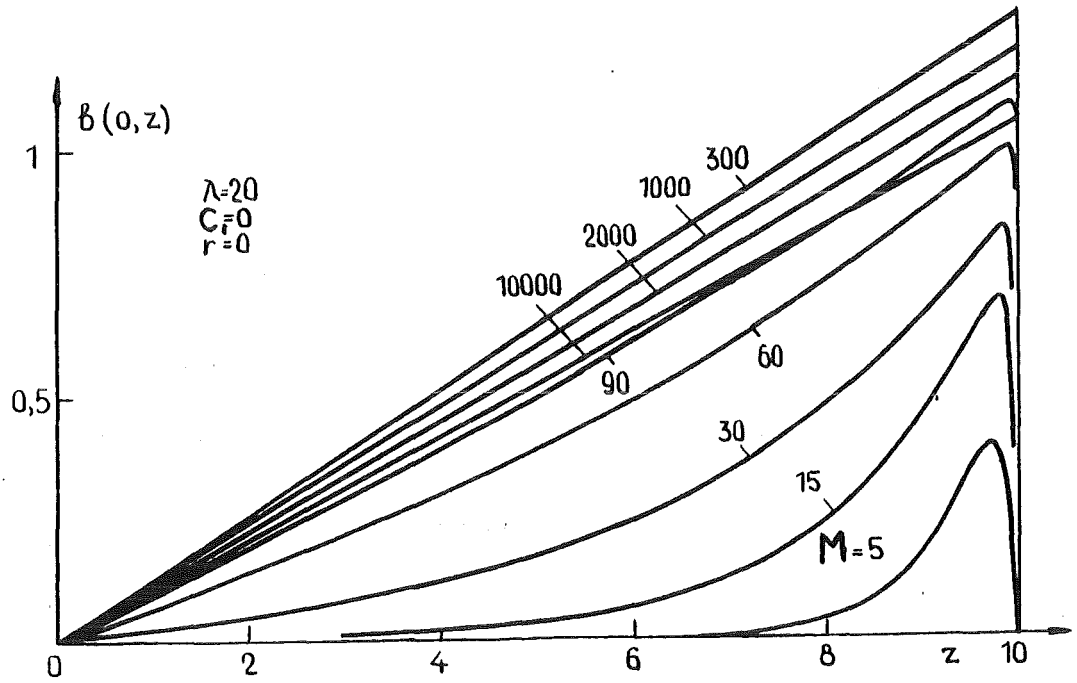

Fig. 3.8 The induced magnetic field in a rectangular slotted channel at the channel axis $y=0$ for different values of the Hartmann number. The Hartmann wall is insulating $(c_1 = 0)$.

The distribution of the induced magnetic field *b(0,z)* in this channel at different values of M is shown in figure 3.8. From this figure it is seen that with increasing Hartmann number the distribution of the electric current density on the channel axis $\left(j_y(0,z) \approx -\frac{\partial b}{\partial z}\right)$ tends to become uniform.

The velocity distribution *v(0,z)* in the channel with conducting Hartmann walls $(\lambda = 20,\ c_1 = 0.01,\ r = 0)$ is shown in figure 3.9. At high M the fluid velocity at the centre of the channel becomes lower than one, so that the profile becomes of M-shape type. The flow structure is shown in more detail in figure 3.10. The comparison of the velocity profiles in channels with $\lambda = 20$ and $\lambda = 50$ shows that for equal values of the parameters M and c_1 the M-shape of the profile appears for lower values of M and is more pronounced in the channel with smaller aspect ratio. It is also shown in the same figures how the flow structure is transformed with the increasing contact resistance r at the Hartmann walls. The appearance of the contact resistance leads at first to evening of the velocity profile along the channel height, and for higher values of r to the suppression of the M-shapeness of the profile.

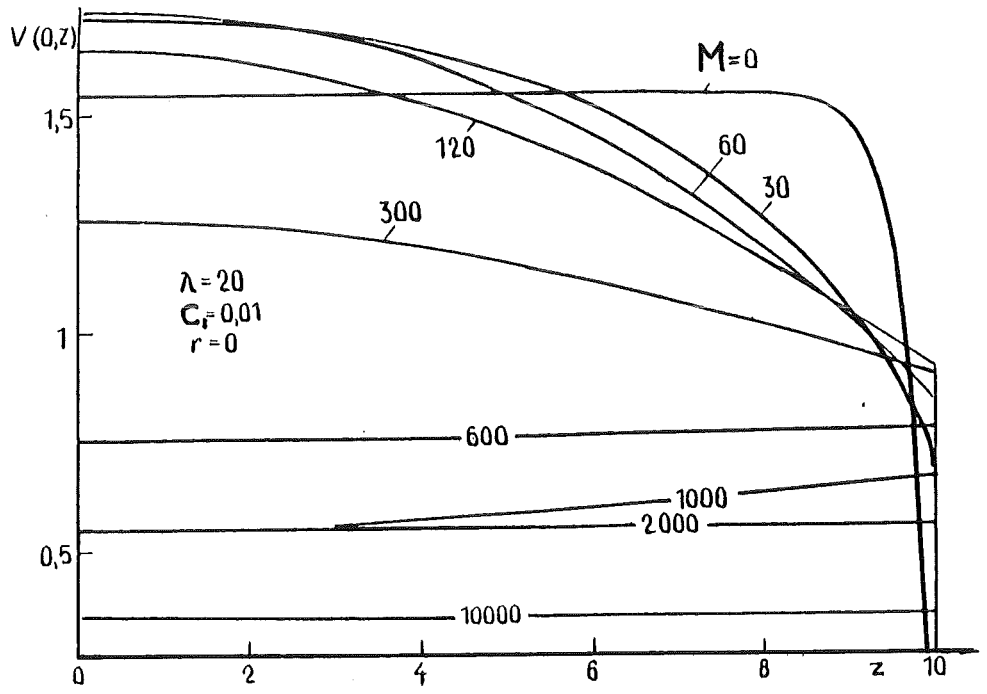

Fig. 3.9 Fluid velocity in a rectangular slotted channel at the channel axis *y=0* for different values of the Hartmann number. The Hartmann wall is electrically conducting .

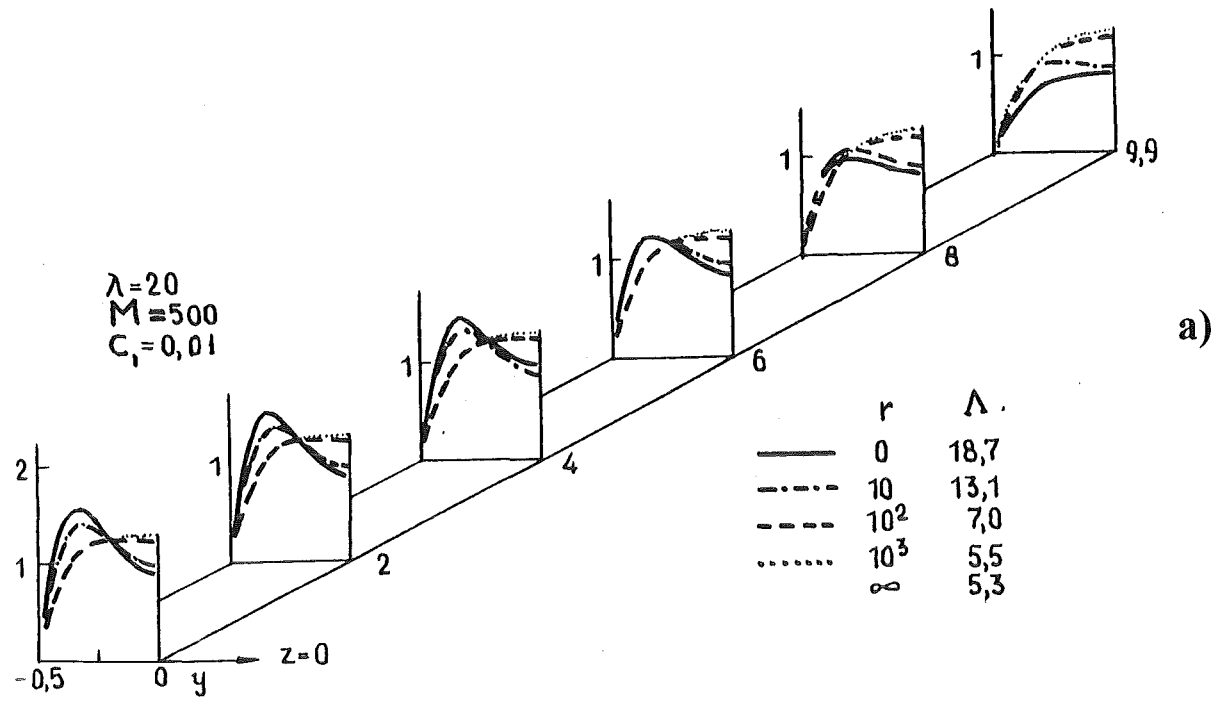

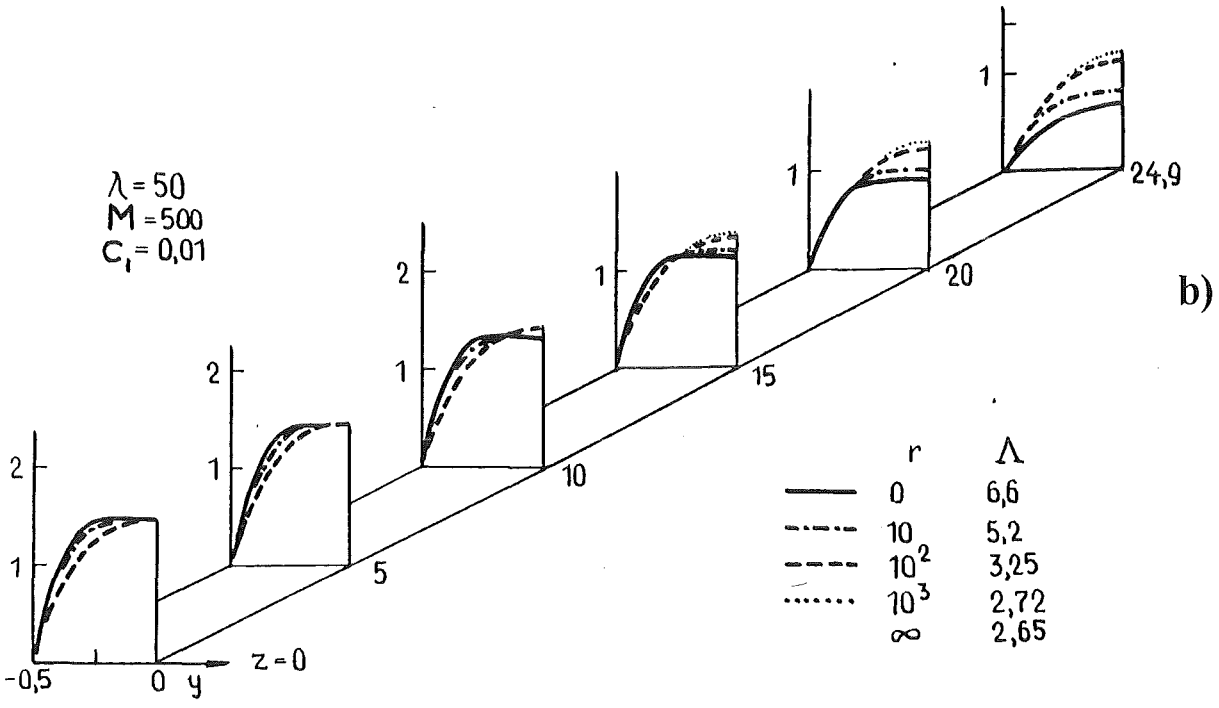

Fig. 3. 10 (a,b) Fluid velocity for different values of λ, M, r and c_1.

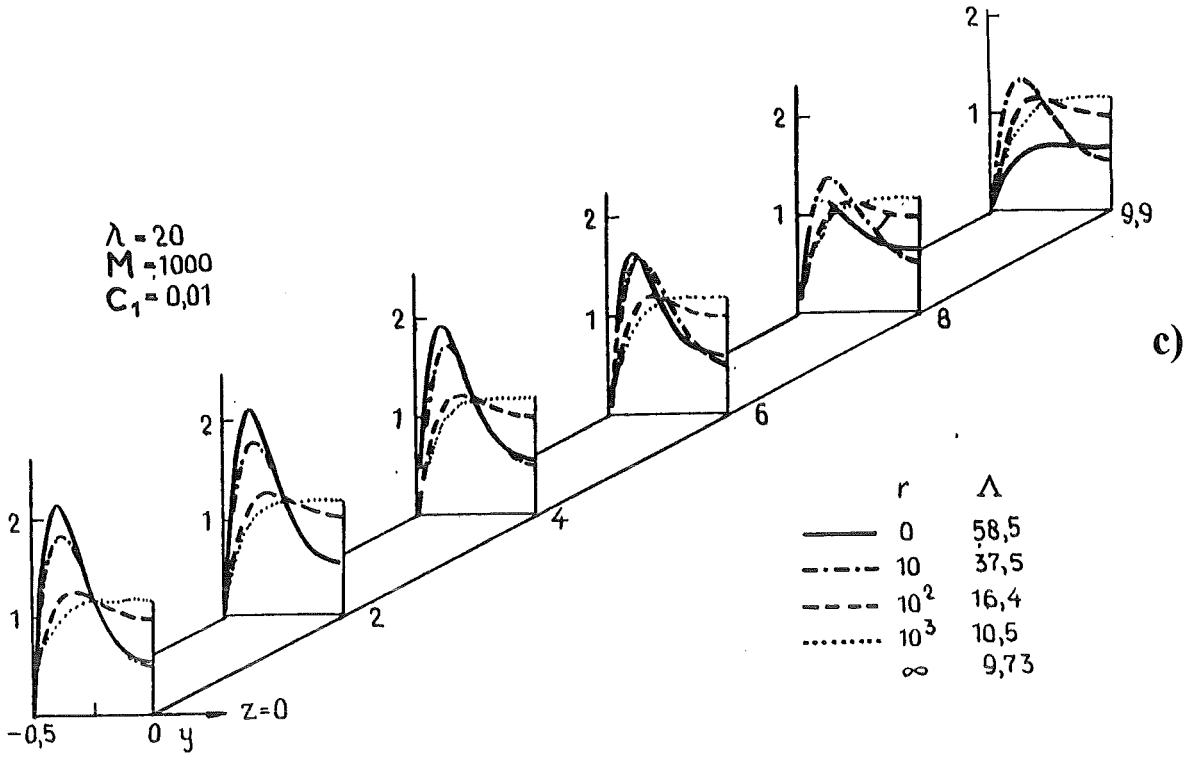

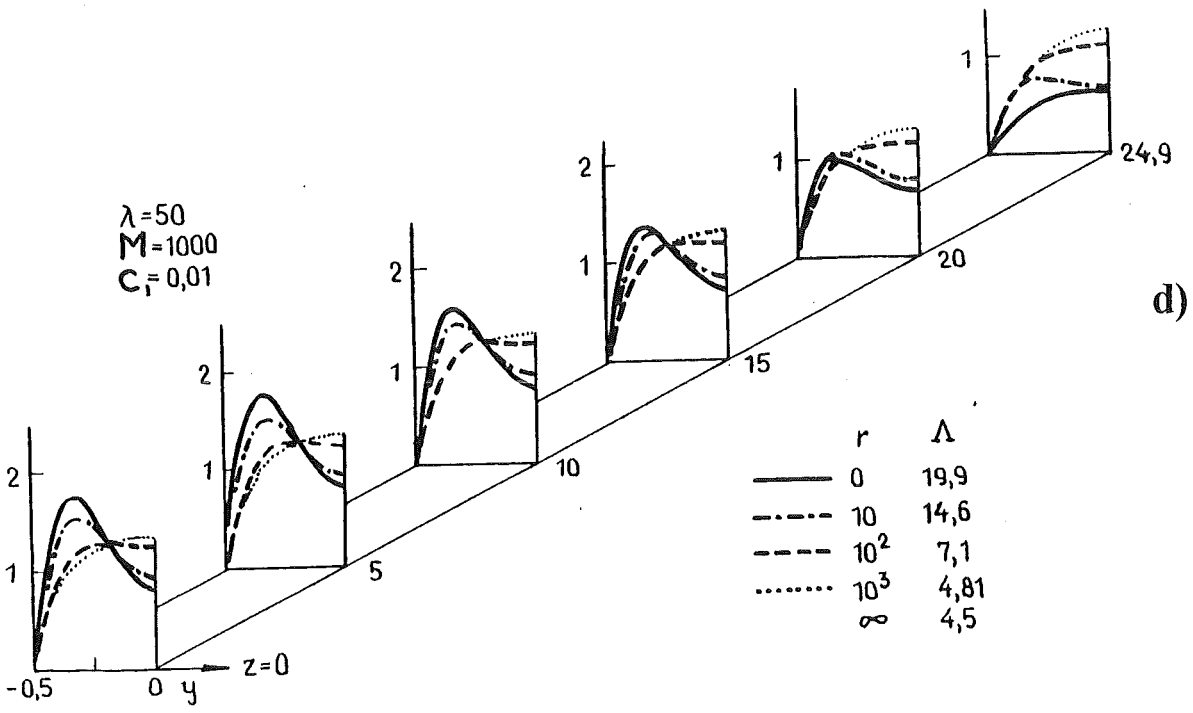

Fig. 3.10 (c,d) Fluid velocity for different values of λ, M, r and c_1.

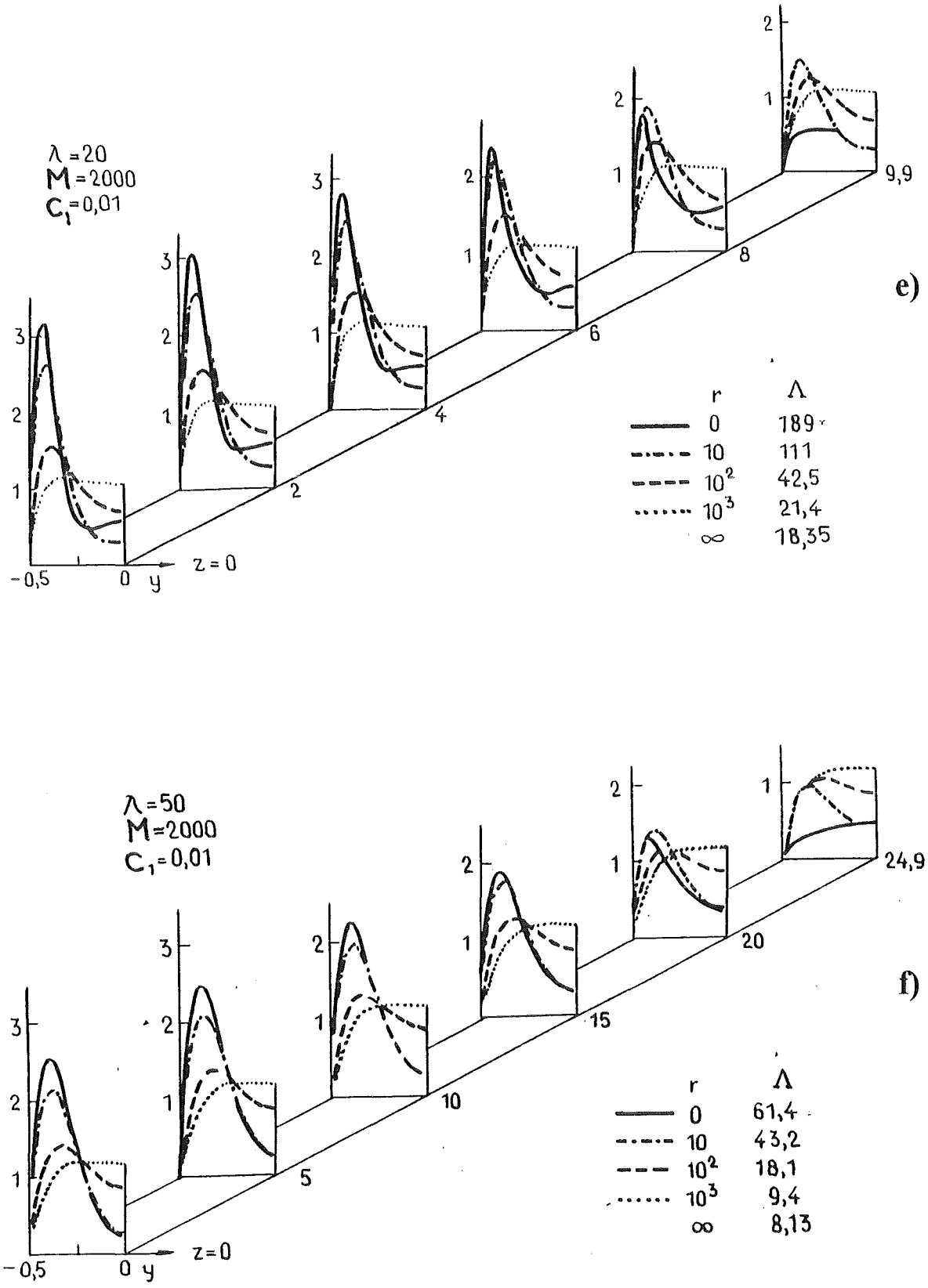

Fig. 3.10 (e,f) Fluid velocity for different values of λ, M, r and c_1.

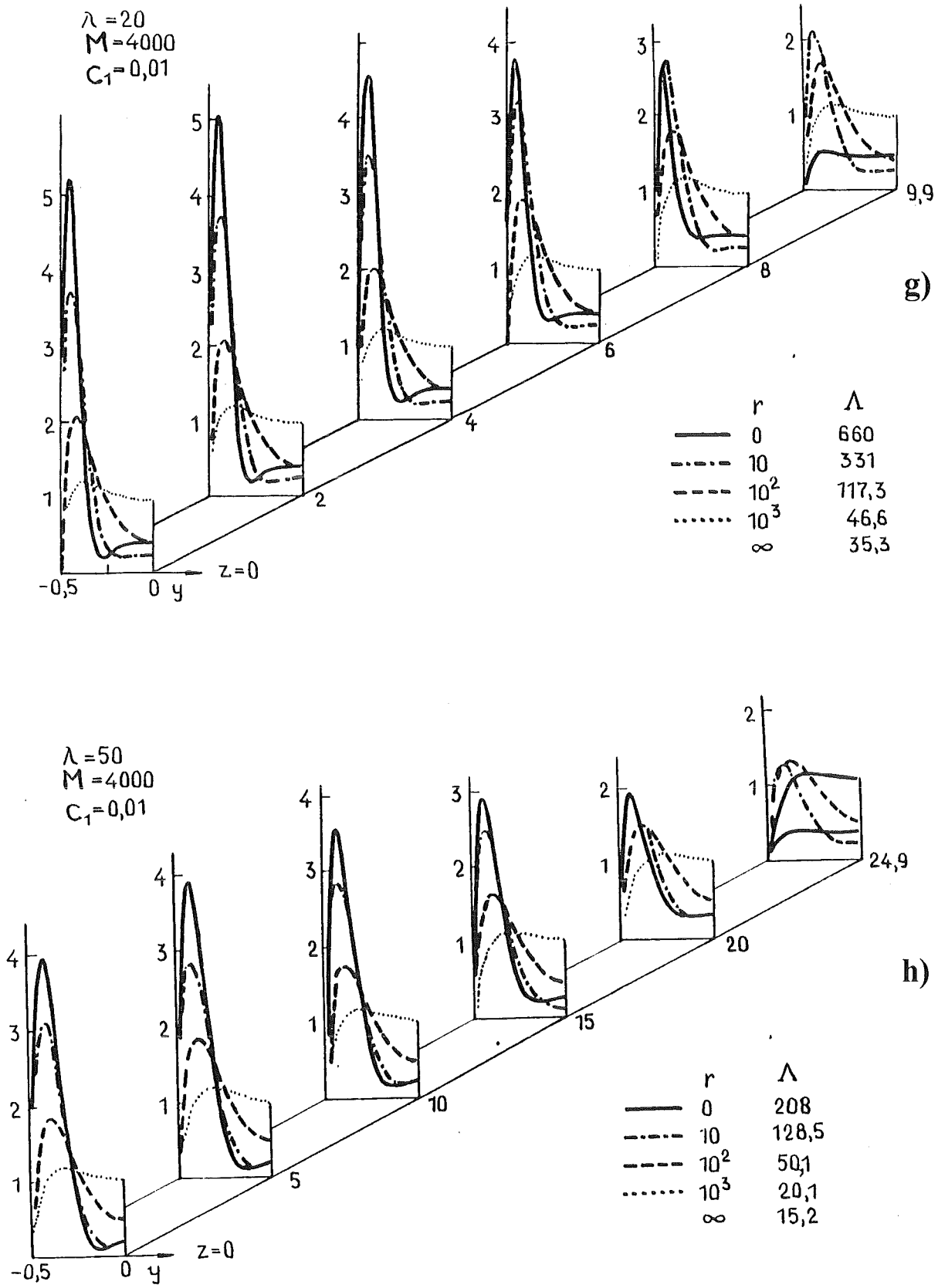

Fig. 3.10 (g,h) Fluid velocity for different values of λ, M, r and c_1.

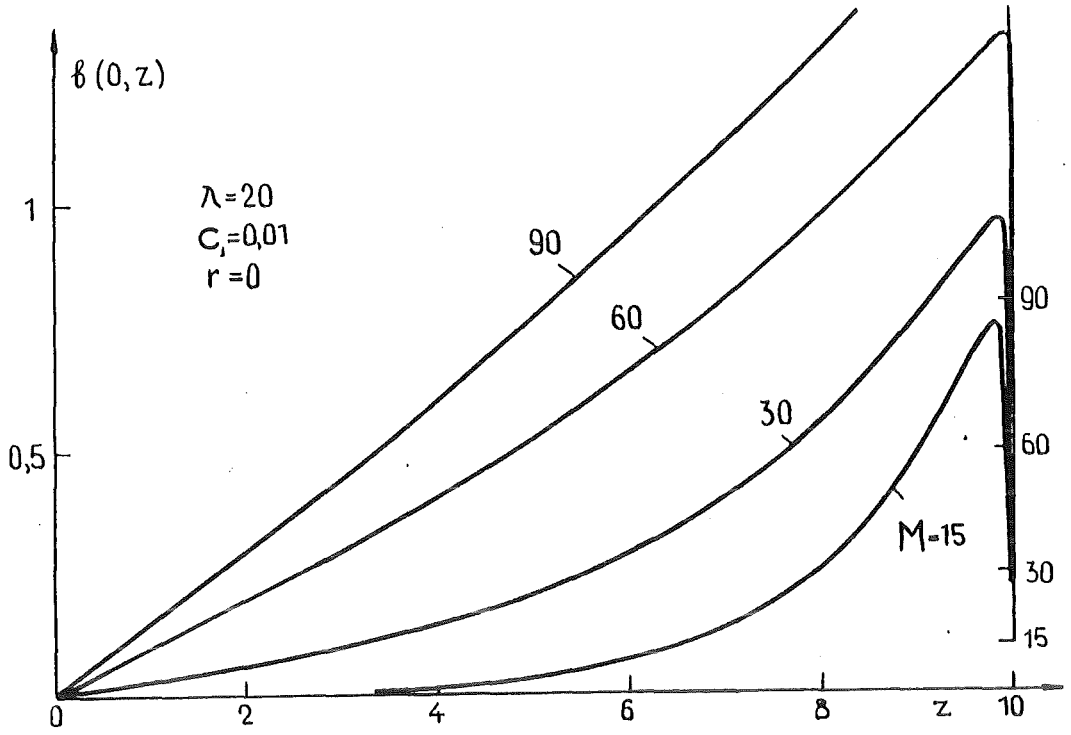

Fig. 3.11 The induced magnetic field in a rectangular slotted channel at the channel axis $y=0$ for different values of the Hartmann number. The Hartmann wall is electrically conducting.

The distribution of the induced magnetic field $b(0,z)$, calculated at certain value of M for the channel with $\lambda = 20$, $c_1 = 10^{-2}$ and $r=0$, is shown in figure 3.11. Similar to the channel with insulating walls the current density $\cong \partial b / \partial z$ becomes uniform with increasing M, and its magnitude monotonically increases. The values of $b(0,10)$ are shown in this figure. With increasing M the electric currents flowing in the Hartmann layer and in the wall redistribute, and more current is conducted by the wall.

Finally we present the relation which allows one to estimate the value of $\Lambda(M, \lambda, c_1, 0)$ with high accuracy for the channel with conducting Hartmann walls, namely

$$\Lambda(M,\lambda,c_1,0) = \frac{2M(1+c_1M)}{P(0,\lambda)(\lambda+2c_1)} \times$$

$$\times\left\{1-\frac{2}{\lambda M}-\left[1+\frac{c_1\lambda M}{4(\lambda+2c_1)}\right]\frac{1.704}{\sqrt{\dfrac{2M(1+c_1M)}{\lambda+2c_1}}}+\frac{c_1\lambda M}{4(\lambda+2c_1)}\frac{2.4}{\sqrt{2M/\lambda}}\right\}^{-1}. \qquad (3.23)$$

4. Conclusions

In poloidal concepts of self-cooled liquid-metal blankets for tokamak reactors the major part of flow is fully developed or almost fully developed. If coolant duct walls are insulating, the ducts have rectangular cross-section, and the magnetic field is parallel to one pair of the duct walls, the bulk of the fluid flows with constant velocity (slug velocity profile). This leads to desirable heat-transfer characteristics. Moreover, in insulating rectangular ducts two-dimensional turbulence may be present at moderate values of the interaction parameter, which may only improve these characteristics.

In the present work the influence of possible deviations from such ideal conditions are estimated. The first part evaluates the effect of non-perfect alignment of the magnetic field with duct walls, while the second part estimates the effect of non-perfect insulation of duct walls, if insulating coatings are used for this purpose.

If the duct cross-section is square or close to it, inclination of the field does not affect seriously both the pressure drop and heat transfer characteristics. The conclusion about the latter is made on the analysis of the laminar velocity profiles presented here. For inclination relevant to fusion applications in the range of 10^o the deviation of the velocity profile from the slug one is insignificant. In case of a square duct the increase of the pressure gradient due to field inclination is negligible (less than 10 per cent for any angle). The pressure drop in a rectangular insulating channel is inversly proportional to channel aspect ratio l and by using slotted channels may be reduced considerably. For very high values of l, however, the increase of the pressure drop due to field inclination and change of the velocity profile, especially close to the corners may lead to undesirable conditions. To avoid this the aspect ratio of the channel should be chosen not very high. In any case the pressure drop in fully developed flow in a duct with insulating walls is proportional to B_0 in contrast to a duct with conducting walls, where it is proportional to B_0^2.

If duct walls are non-perfectly isolated, the appearance of the contact resistance leads at first to the evening of the velocity profile along the channel height and then to the suppression of the M-shapeness. More details about this question are given by Bühler & Molokov (1993).

References

Bühler, L. & Molokov, S. *1993* Magnetohydrodynamic flows in ducts with insulating coatings. *Kernforschungszentrum Karlsruhe. Report KfK-5103.*

Kevorkian, L. & Cole, J.D. *1981 Perturbation Methods in Applied Mathematics.* Springer-Verlag.

Lavrentiev, I.V. *1990* Liquid-metal systems in tokamak thermonuclear reactors. *Magnetohydrodynamics.* **26** (2), 227-245.

Malang, S., Bojarsky, E., Bühler, L., Deckers, H., Fischer, U., Norajitra, P. & Reiser, H. *1993* Dual coolant liquid metal breeder concept. *Proc. 17th Symposium on Fusion Technology, Rome, Italy, 14-18 September 1992,* vol. **2**, 1424-1428.

Molokov, S. *1990* Magnetohydrodynamic flow in a rectangular channel in a strong skewed magnetic field. *Proc. 13th Riga Conference on Magnetohydrodynamics,* Riga 1990, Pt. 1, pp. 23-24 (In Russian).

Shercliff, J.A. *1953* Steady motion of conducting fluids in pipes under transverse magnetic fields. *Proc. Cambr. Philos. Soc.* **49**, pp. 136-144.

Shercliff, J.A. *1956* The flow of conducting fluids in circular pipes under transverse magnetic fields. *J.Fluid Mech.* **1** (6), pp. 644-666.

Shercliff, J.A. *1965 A Textbook of Magnetohydrodynamics.* Longmans.

Sze, D.K., Mattas, R.F., Hull, A.B., Picologlou, B. & Smith, D.L. *1992* MHD considerations for a self-cooled liquid lithium blanket. *Fusion Technology.* **21** (3), Pt 2b, 2099-2106.

Temperley D.J. *1976* Magnetohydrodynamic flow in a rectangular duct under a uniform transverse magnetic field at high Hartmann number. *Archives of Mechanics.* **28** (5-6), 947-968.

Vatazhin, A.B., Liubimov, G.A. & Regirer, S.A. *1970 Magnetohydrodynamic Channel Flows.* Moscow, Nauka (In Russian).

Appendix A

Values of function $\Lambda(M, \lambda, c_1, r)$

M=500

	λ	10	20	30	40	50
c_1	r					
0		9.41	5.32	3.86	3.11	2.65
10^{-4}		9.8	5.51	3.98	3.2	2.72
$5 \cdot 10^{-4}$		11.33	6.27	4.47	3.55	2.99
10^{-3}		13.19	7.19	5.06	3.97	3.3
$5 \cdot 10^{-3}$		26.14	13.27	8.8	6.53	5.18
10^{-2}	0	38.75	18.7	11.93	8.57	6.6
	10	25.07	13.09	8.75	6.52	5.2
	100	12.76	7.02	4.96	3.9	3.25
	1000	9.79	5.51	3.98	3.2	2.72
$2 \cdot 10^{-2}$	0	56.55	25.67	15.7	10.9	8.15
	10	29.03	15.02	9.92	7.3	5.74
	100	12.91	7.1	5	3.93	3.28
	1000	9.79	5.51	3.98	3.2	2.72
$4 \cdot 10^{-2}$	0	77.14	32.83	19.31	13	9.5
	10	31.87	16.4	10.75	7.85	6.11
	100	12.99	7.14	5.03	3.95	3.3
	1000	9.8	5.51	3.98	3.2	2.72
$6 \cdot 10^{-2}$	0	88.7	36.49	21.05	13.98	10
	10	33.02	16.95	11.07	8.06	6.26
	100	13.02	7.15	5.04	3.96	3.3
	1000	9.8	5.51	3.98	3.2	2.72

M=1000

	λ	10	20	30	40	50
c_1	r					
0		17.75	9.73	6.87	5.4	4.5
10^{-4}		19.32	10.53	7.4	5.8	4.81
$5 \cdot 10^{-4}$		25.44	13.63	9.45	7.3	6
10^{-3}		32.77	17.3	11.84	9.05	7.35
$5 \cdot 10^{-3}$		81.64	40	26	19	14.83
10^{-2}	0	125.7	58.54	36.68	26.1	19.9
	10	72.1	37.54	25.07	18.6	14.6
	100	30.32	16.36	11.32	8.71	7.1
	1000	19.24	10.5	7.4	5.8	4.81
$2 \cdot 10^{-2}$	0	182.7	79.92	48.21	33.4	24.94
	10	83.54	43.35	28.8	21.23	16.6
	100	30.86	16.65	11.52	8.85	7.2
	1000	19.25	10.5	7.4	5.8	4.81
$4 \cdot 10^{-2}$	0	242	99.62	58.14	39.4	28.92
	10	91.3	47.28	31.3	22.98	17.9
	100	31.15	16.8	11.62	8.93	7.3
	1000	19.25	10.5	7.4	5.8	4.81
$6 \cdot 10^{-2}$	0	272.5	108.9	62.6	42	30.6
	10	94.3	48.8	32.26	23.65	18.4
	100	31.95	16.85	11.66	8.8	7.3
	1000	19.25	10.5	7.4	5.8	4.81

M=1500

λ		10	20	30	40	50
c_1	r					
0		26	14	9.83	7.66	6.33
10^{-4}		29.5	15.9	11.04	8.56	7.05
$5\cdot10^{-4}$		43.2	22.8	15.65	12	9.75
10^{-3}		59.46	30.9	20.95	15.9	12.78
$5\cdot10^{-3}$		164.5	79.34	50.86	36.84	28.6
10^{-2}	0	254.2	116	71.77	50.62	38.45
	10	135.9	70.6	47.1	35	27.6
	100	52.62	28.27	19.5	14.9	12.1
	1000	29.24	15.8	11	8.55	7.04
$2\cdot10^{-2}$	0	363.8	156	92.97	63.91	47.62
	10	156.2	80.96	53.8	39.8	31.2
	100	53.72	28.86	19.9	15.2	12.4
	1000	29.26	15.8	11	8.55	7.04
$4\cdot10^{-2}$	0	470.1	190.6	110.2	74.21	54.5
	10	169.5	87.72	58.13	42.86	33.5
	100	54.3	29.17	29.17	20.12	15.4
	1000	29.27	15.8	11	8.55	7.04
$6\cdot10^{-2}$	0	523	206.3	117.6	78.54	57.32
	10	174.5	90.3	59.8	44	34.4
	100	54.5	29.28	20.19	15.4	12.5
	1000	29.27	15.8	11	8.55	7.04

M=2000

	λ	10	20	30	40	50
c_1	r					
0		34.14	18.35	12.76	9.88	8.13
10^{-4}		40.4	21.57	14.92	11.5	9.42
$5 \cdot 10^{-4}$		64.6	33.87	23.08	17.57	14.2
10^{-3}		93.2	48.1	32.34	24.35	19.5
$5 \cdot 10^{-3}$		273	130.1	82.7	59.5	45.9
10^{-2}	0	420.1	189.1	116	81.26	61.42
	10	213.7	110.9	73.9	54.8	43.2
	100	79.1	42.42	29.23	22.37	18.14
	1000	39.84	21.4	14.83	11.45	9.39
$2 \cdot 10^{-2}$	0	592.2	250.6	148.2	101.3	75.17
	10	243.8	126.3	83.8	61.93	48.63
	100	80.8	43.38	29.9	22.87	18.54
	1000	39.87	21.4	14.84	11.46	9.4
$4 \cdot 10^{-2}$	0	752.4	301.6	173.3	116.3	85.1
	10	263	136.1	90.1	66.41	52
	100	125	81.74	43.88	30.24	18.76
	1000	39.88	21.4	14.84	11.47	9.4
$6 \cdot 10^{-2}$	0	828.6	324	183.9	122.4	89.1
	10	270.2	139.7	92.45	68.1	53.3
	100	82.06	44.06	30.36	23.23	18.8
	1000	39.89	21.41	14.85	11.47	9.4

M=2500

c_1	r \ λ	10	20	30	40	50
0		42.26	22.6	15.66	12.1	9.92
10^{-4}		52	27.64	19	14.63	11.94
$5\cdot10^{-4}$		89.7	46.75	31.72	24.05	19.4
10^{-3}		133.4	68.65	45.97	34.5	27.55
$5\cdot10^{-3}$		405.7	191.5	121	86.7	66.6
10^{-2}	0	620	276.3	168.3	117.4	88.41
	10	304	157.6	104.9	77.7	61.22
	100	109.2	58.56	40.34	30.9	25
	1000	51	27.3	18.86	14.52	11.88
$2\cdot10^{-2}$	0	862.7	361.5	212.7	144.8	107.1
	10	344	178.3	118.3	87.3	68.5
	100	111.7	59.93	41.29	31.6	25.6
	1000	51	27.3	18.87	14.53	11.88
$4\cdot10^{-2}$	0	1081	430	246.2	164.7	120.2
	10	370	191.3	126.6	93.3	73
	100	113	60.65	41.79	32	25.9
	1000	51	27.3	18.88	18.88	11.89
$6\cdot10^{-2}$	0	1182	459.4	260	172.7	125.5
	10	379	196.1	129.7	95.45	74.68
	100	113.5	60.9	41.96	32.1	26
	1000	51.1	27.3	18.88	14.34	11.89

M=500

	λ	10	20	30	40	50
c_1	r					
$8 \cdot 10^{-2}$	0	96.1	38.71	22.08	14.54	10.4
	10	33.63	17.24	11.25	8.17	6.34
	100	13.03	7.16	5.05	3.96	3.3
	1000	9.8	5.51	3.98	3.2	2.72
0.1	0	101	40.2	27.76	14.91	10.7
	10	34	17.43	11.36	8.24	6.39
	100	13.04	7.16	5.05	3.96	3.3
	1000	9.8	5.51	3.98	3.2	2.72
0.5	0	122.7	46.02	25.32	16.27	11.5
	10	35.33	18.06	11.73	8.48	6.56
	100	13.07	7.18	5.06	3.97	3.31
	1000	9.8	5.51	3.98	3.2	2.72
1	0	126.2	46.89	25.69	16.46	11.6
	10	35.5	18.14	11.78	8.52	6.58
	100	13.07	7.18	5.06	3.97	3.31
	1000	9.8	5.51	3.98	3.2	2.72
5	0	129.1	47.61	26	16.62	11.7
	10	35.65	18.21	11.82	8.54	6.6
	100	13.08	7.18	5.06	3.97	3.3
	1000	9.8	5.51	3.98	3.2	2.72
10	0	129.4	47.7	26.03	16.64	11.7
	10	35.67	18.22	11.82	8.55	6.65
	100	13.08	7.18	5.06	3.97	3.31
	1000	9.8	5.51	3.98	3.2	2.72

M=1000

	λ	10	20	30	40	50
c_1	r					
$8 \cdot 10^{-2}$	0	291	114.3	65.13	43.46	31.56
	10	95.9	49.6	32.77	24	18.6
	100	31.3	16.88	11.68	8.97	7.3
	1000	19.25	10.5	7.4	5.8	4.81
0.1	0	303.6	117.8	66.77	44.4	32.15
	10	96.88	50.11	33.1	24.23	18.8
	100	31.33	16.9	11.69	8.98	7.31
	1000	19.25	10.5	7.4	5.8	4.81
0.5	0	352.7	131	72.68	47.72	34.26
	10	100	51.8	34.15	24.97	19.3
	100	31.43	16.95	11.72	9	7.33
	1000	19.25	10.5	7.4	5.8	4.82
1	0	360	133	73.5	48.17	34.54
	10	101	52	34.3	25.06	19.4
	100	31.44	16.95	11.73	9.01	7.33
	1000	19.25	10.5	7.4	5.8	4.82
5	0	366.2	134.4	74.2	48.55	34.77
	10	101	52.2	34.4	25.14	19.5
	100	31.46	16.96	11.73	9.01	7.34
	1000	19.25	10.5	7.4	5.8	4.82
10	0	367	134.4	74.26	48.6	34.8
	10	101	52.22	34.42	25.15	19.5
	100	31.46	16.96	11.73	9.01	7.34
	1000	19.25	10.5	7.4	5.8	4.82

M=1500

	λ	10	20	30	40	50
c_1	r					
$8 \cdot 10^{-2}$	0	554	215.2	121.7	80.92	58.86
	10	177.2	91.64	60.64	44.6	34.9
	100	54.6	29.34	20.23	15.5	12.6
	1000	29.27	15.8	11	8.55	7.04
0.1	0	574.6	220.9	124.4	82.43	59.83
	10	178.8	92.48	61.48	45	35.2
	100	54.66	29.37	20.25	15.5	12.6
	1000	29.27	15.8	11	8.55	7.04
0.5	0	652.9	241.7	133.7	87.7	63.2
	10	184.3	95.27	62.27	46.3	36.1
	100	54.85	29.48	20.32	15.55	12.6
	1000	29.27	15.8	11	8.55	7.04
1	0	664.3	244.6	135	88.4	63.64
	10	185	95.63	63.2	46.4	36.2
	100	54.88	29.49	20.33	15.6	12.6
	1000	29.27	15.8	11	8.55	7.04
5	0	673.7	247	136	89	64
	10	185.6	95.93	63.4	46.6	36.3
	100	54.9	29.5	20.34	15.6	12.6
	1000	29.28	15.8	11	8.55	7.04
10	0	674.9	247.3	136.2	89.1	64.06
	10	185.7	95.97	63.4	46.6	36.3
	100	54.9	29.5	20.34	15.6	12.6
	1000	29.28	15.8	11	8.55	7.04

M=2000

	λ	10	20	30	40	50
c_1	r					
$8 \cdot 10^{-2}$	0	872.6	336.5	189.7	125.7	91.25
	10	274	141.6	93.68	68.96	53.94
	100	82.22	44.14	30.42	23.28	18.86
	1000	39.89	21.41	14.85	11.47	9.4
0.1	0	901.7	344.5	19.34	127.7	92.6
	10	276	142.8	94.44	69.5	54.35
	100	82.32	44.2	30.45	23.3	18.89
	1000	39.9	21.41	14.85	11.47	9.4
0.5	0	1010	373.3	206.4	135.1	97.24
	10	284	146.8	97	71.3	55.7
	100	82.63	44.37	30.58	23.4	19
	1000	39.9	21.41	14.85	11.47	9.4
1	0	1025	377.3	208.1	136.1	97.86
	10	285	147.3	97.3	71.5	55.86
	100	82.67	44.39	30.59	23.4	19
	1000	39.9	21.41	14.85	11.47	9.4
5	0	1038	380.5	209.5	136.9	98.34
	10	286	147.7	97.5	71.7	56
	100	82.7	44.41	30.6	23.4	19
	1000	39.9	21.41	14.85	11.47	9.4
10	0	1040	380.9	209.7	137	98.42
	10	286	147.7	97.6	71.7	56
	100	82.7	44.41	30.6	23.4	19
	1000	39.9	21.41	14.85	11.47	9.4

M=2500

	λ	10	20	30	40	50
c_1	r					
$8 \cdot 10^{-2}$	0	1239	475.6	267.6	177	128.3
	10	384	198.6	131.3	96.6	75.53
	100	113.7	61.02	42.05	32.2	26.1
	1000	51.1	27.3	18.9	14.54	11.89
0.1	0	1277	486	272.3	180	130
	10	387	200.1	132.3	97.3	76.1
	100	113.8	61.1	42.1	32.2	26.1
	1000	51.1	27.3	18.9	14.55	11.89
0.5	0	1416	522.8	288.9	189.1	136
	10	397	205.2	135.5	99.6	77.8
	100	114.2	61.33	42.27	32.3	26.2
	1000	51.1	27.3	18.9	14.55	11.89
1	0	1436	527.8	291.1	190	136.7
	10	398	205.9	136	100	78
	100	114.3	61.37	42.29	32.4	26.2
	1000	51.1	27.3	18.9	14.55	11.89
5	0	1452	532	292.9	191	137.4
	10	399.5	206.4	136.3	100.1	78.2
	100	114.3	61.39	42.31	32.4	26.25
	1000	51.1	27.3	18.9	14.55	11.89
10	0	1454	532.4	293.1	191.5	137.5
	10	399.6	206.5	136.3	100.2	78.23
	100	114.4	61.39	42.31	32.4	26.25
	1000	51.1	27.3	18.9	14.55	11.89